Re-revised manuscript

Persistence of the mitochondrial permeability transition in the absence of subunit c of human ATP synthase

Jiuya He, Holly C. Ford, Joe Carroll, Shujing Ding, Ian M. Fearnley and John E. Walker

The Medical Research Council Mitochondrial Biology Unit, Cambridge Biomedical Campus, Hills Road, Cambridge CB2 0XY, United Kingdom

*To whom correspondence should be addressed. J. E. W., Tel.: +44-1223-252701; e-mail: walker@mrc-mbu.cam.ac.uk

Running title: The mitochondrial permeability transition pore

The authors declare no conflict of interest

Author contributions: J. E. W. designed research and supervised project; J. H., H. F., J. C., S. D. and I. M. F. performed research; J. H., H. F., J. C., S. D., I. M. F. and J. E. W. analysed data, and J. E. W. prepared the manuscript

Classification: BIOLOGICAL SCIENCES, Biochemistry

Key words: human mitochondria; ATP synthase; permeability transition pore; subunit c

Abstract

The permeability transition in human mitochondria refers to the opening of a non-specific channel, known as the permeability transition pore (PTP) in the inner membrane. Opening can be triggered by calcium ions, leading to swelling of the organelle, disruption of the inner membrane and ATP synthesis, followed by cell death. Recent proposals suggest that the pore is associated with the ATP synthase complex, and specifically with the ring of c-subunits that constitute the membrane domain of the enzyme's rotor. The c-subunit is produced from three nuclear genes, ATP5G1, ATP5G2 and ATP5G3, encoding identical copies of the mature protein with different mitochondrial targeting sequences that are removed during their import into the organelle. To investigate the involvement of the c-subunit in the PTP, we generated a clonal cell, HAP1-A12, from near-haploid human cells, in which ATP5G1, ATP5G2 and ATP5G3 were disrupted. The HAP1-A12 cells are incapable of producing the c-subunit, but they preserve the characteristic properties of the PTP. Therefore, the c-subunit does not provide the PTP. The mitochondria in HAP1-A12 cells assemble a vestigial ATP synthase, with intact F_1-catalytic and peripheral stalk domains and supernumerary subunits e, f and g, but lacking membrane subunits ATP6 and ATP8. The same vestigial complex plus associated c-subunits was characterized from human 143B ρ^0 cells, which cannot make subunits ATP6 and ATP8, but retain the PTP. Therefore, none of the membrane subunits of the ATP synthase that are involved directly in transmembrane proton translocation is involved in forming the PTP. (246 words).

Significance

Cellular power houses called mitochondria generate fuel known as adenosine triphosphate, or ATP, to sustain complex life. The capacity of mitochondria to do so depends on a supply of energy from oxidation of energy rich compounds in food-stuffs to generate a chemical potential

difference for hydrogen ions, called the proton motive force (pmf), across the inner of their two membranes. Disruption of this membrane dissipates the pmf, and the cells die for lack of fuel. This event happens, for example, when the concentration of calcium ions inside human mitochondria is increased. The mitochondria respond by opening a pore, water enters, the mitochondria swell and burst. The molecular identity of the pore is disputed, and we have disproved one proposal. (119 words)

Introduction

The inner membranes of mitochondria contain a high conductance non-specific channel, known as the permeability transition pore (or PTP), which opens in response to elevated concentrations of Ca^{2+} in the mitochondrial matrix (1). Opening of the pore is potentiated by inducers such as phosphate, adenine nucleotide depletion and thiol oxidants, and leads to the swelling of the mitochondria, loss of proton motive force (pmf), disruption of ion homeostasis and hydrolysis of ATP by the ATP synthase (2). These events have been linked to pathways leading to cell death, and to human diseases including cardiac ischemia and muscle dystrophy (3). The opening of the pore can be induced artificially by compounds such as thapsigargin, a non-competitive inhibitor of the Ca^{2+}-ATPase in the sarcoplasmic and endoplasmic reticula (4), and by ionophores for divalent cations such as ferutinin (5). It can also be inhibited by drugs such as cyclosporin A, mediated via its binding to the prolyl cis-trans isomerase, cyclophilin D, in the mitochondrial matrix (6, 7).

Since the discovery of the mitochondrial permeability transition, many proposals have been made about the protein constituents of the PTP itself, including the ADP/ATP translocase, an abundant component of the inner membranes of mitochondria, and the voltage dependent anion channel found in the outer membranes of the organelle, but none of these proposals has been established definitively (8, 9). Recently, it has been proposed that the PTP is associated

with another abundant component of the inner mitochondrial membrane, the ATP synthase complex (10). The monomeric mammalian ATP synthase is a multiprotein assembly made of eighteen different protein subunits (11). The enzyme consists of two major domains, a membrane intrinsic sector and a membrane extrinsic F_1-sector, joined together by central and peripheral stalks (11). In mitochondria, the monomeric complexes form dimers via interactions between their membrane domains, and the dimers associate in rows along the edges of the cristae (12, 13). The membrane domain of each monomer contains a rotary motor driven by the pmf produced by respiration. The membrane embedded part of the rotor is a ring of eight c-subunits in the bovine enzyme (14). Since the sequences of the bovine and human c-subunits are identical, it is reasonable to assume that the human c-ring is identical. In the intact enzyme, the external surface of this ring is in contact with a single ATP6 (or a) subunit (15–18). During ATP synthesis, the c_8-ring turns with estimated speeds of up to 300 Hz. The generation of rotation involves the translocation of protons across the membrane domain of the enzyme via a pathway at the interface between the surface of the c-ring and subunit ATP6. The rotational energy of the rotor is transmitted to the catalytic domain by the central stalk, which is a membrane extrinsic structure attached firmly to the c-ring. The central stalk consists of single copies of the γ-, δ- and ε-subunits and lies along the central axis of the F_1 domain, surrounded by the $\alpha_3\beta_3$-catalytic domain, a hexameric structure of alternating α- and β-subunits. At three of the six α-β-interfaces are found the catalytic sites of the enzyme, where ATP is formed from ADP and inorganic phosphate, using energy supplied by rotation (19, 20). In the absence of a proton-motive force, the F_1-ATPase inhibitor protein, IF_1, prevents the hydrolysis of ATP by binding to one of the catalytic interfaces (21). The main role of the peripheral stalk, a predominantly α-helical structure made from single copies of the oligomycin sensitivity conferral protein (OSCP), and subunits b, d and factor 6 (F_6) (22–24) is to link the $\alpha_3\beta_3$ domain to subunit ATP6, which interacts with the two predicted trans-membrane α-helices of the b-

subunit, so that together the $\alpha_3\beta_3$ domain, the peripheral stalk and subunit a form the stator of the enzyme (11, 18). The membrane domain of the mammalian ATP synthase also contains six other proteins e, f, g, DAPIT (diabetes associated protein in insulin sensitive tissues), 6.8PL (6.8 kDa proteolipid) and ATP8 (or A6L) (25–29). They are known collectively as the "supernumerary" subunits, and with the exception of ATP8, they appear to have no direct role in the synthesis of ATP. They are all localised in the vicinity of the region of interaction between monomers in the dimeric complex. Each is predicted to contain a single transmembrane α-helical span (30). Subunits ATP6 and ATP8 are the only components of the complex that are encoded in the mitochondrial genome (25); all the other subunits of the human complex are the products of single nuclear genes, except for subunit c which is encoded by three genes, ATP5G1, ATP5G2 and ATP5G3 (31, 32) (Fig. S1). Their gene products differ only in the sequences of their N-terminal regions, which direct the protein from the cellular cytoplasm to the inner mitochondrial membrane, and are removed by proteolysis to generate the same identical mature c-subunit found assembled in ATP synthase complexes.

If the PTP is associated with the ATP synthase complex, it is likely that it will involve one or more of the membrane subunits, and one proposal that has been made is that the c_8-ring of the human ATP synthase provides the mitochondrial PTP (33–35). In order to test this proposal, as described here, we have disrupted ATP5G1, ATP5G2 and ATP5G3 together in a single clone of a near-haploid human cell line, and investigated whether the PTP, which is present in the parent HAP1 cells, persists in the mutant cells devoid of subunit c.

Results

Characteristics of wild-type HAP1 cells. HAP1 cells have a haploid karyotype except for a fragment of chromosome 15 which is located in chromosome 19, and they also contain a reciprocal translocation between chromosomes 9 and 22 (36, 37). None of these features affects

the structures of the three genes ATP5G1, ATP5G2 and ATP5G3 encoding the three different precursors of the c-subunit of ATP synthase, which are found, respectively, on the single copy chromosomes 17, 12 and 2. All three genes are transcribed in HAP1 cells, but ATPG3 is expressed predominantly with about 75% of the transcripts arising from this gene (Fig. S2).

Human cells devoid of subunit c. In a clonal HAP1 cell line the ATP5G1, ATP5G2 and ATP5G3 genes were disrupted. Three pairs of guide RNAs (gRNAs), each pair specific for one of the exons IV in ATP5G1 or ATP5G2, or for exon III in ATP5G3, were introduced together into the cells (Fig. S1; Table S1). Clones arising from single cells, identified as having expressed Cas9, were screened for the presence of the c-subunit by western blotting. By this means, clone HAP1-A12 was found to be devoid of subunit c (Fig. 1). Analysis of DNA sequences (Table S2) in regions of its genome where ATP5G1 and ATP5G2 are found showed that deletions of 140 and 97 bases, respectively, had been introduced into exons IV in ATP5G1 and ATP5G2 (Fig. S3A and B). Each had arisen from two gRNAs and non-homologous end-joining (NHEJ) (38) of the deleted genomic DNA. The deletion in ATP5G1 changed the sequence of the precursor of subunit c immediately before the precursor cleavage site and introduced an unrelated sequence of eighteen amino acids which then terminated, and that in ATP5G2 changed the frame of the coding region in the import sequence, leading to an altered protein sequence four amino acids before the junction with the mature protein, and truncation of the frame-shifted protein nine amino acids thereafter. Sequencing of ATP5G3 showed that gRNA ATP5G3-1 had been targeted successfully to the gene whereas ATP5G3-2 had not (Table S1), and a four base deletion had been introduced into the gene by NHEJ. This deletion changed the frame of the encoded protein in the import precursor region, producing a frame shifted protein ten amino acids before the junction between the import sequence and the mature protein, which terminated fourteen amino acids later (Fig. S3C). Thus, none of the three disrupted genes in the HAP1-A12 clone was capable of producing a protein containing any of

the sequence of the mature c-subunit.

Characteristics of HAP1-A12 cells. The co-disruption of ATP5G1, ATP5G2 and ATP5G3 and the accompanying removal of the c-subunit, slightly diminished the ability of the HAP1-A12 cells to grow relative to the wild-type cells (Fig. 2A), and it was accompanied by an increase in the copy number of mitochondrial DNA molecules by about 50% (Fig. 2B). However, the HAP1-A12 cells have a lower respiratory activity (Fig. 2C), which is sufficient to allow them to maintain a mitochondrial membrane potential in the absence of an active ATP synthase (Figs. 2D and 2E). The mitochondria respire using the substrates glutamate/malate and succinate, confirming the presence of active respiratory complexes. The lower initial TMRM signal for HAP1-A12 sample suggests that the mitochondria may be less leaky to protons in the absence of the c-subunit, such that a partial membrane potential can be maintained during the preparation. As expected, there was no impact of oligomycin on either respiration or the membrane potential in HAP1-A12 cells.

The mitochondria of wild-type HAP1 cells and HAP1-A12 cells were stained to the same extent with both TMRM and calcein (Fig. S4) allowing treated cells to be normalised with untreated wild-type cells in subsequent experiments. In order to verify that the mitochondria of HAP1 wild-type cells contain a PTP, the opening of the pore was demonstrated in intact cells in the presence of both thapsigargin and the calcium ionophore ferutinin. For both reagents, the optimum conditions leading to complete opening of the PTP were established (Fig. 3A). With both reagents, the opening of the PTP was prevented by cyclosporin A. Similar results were obtained with HAP1-A12 cells (Fig. 3B). In other experiments with HAP1 and HAP1-A12 cells where their plasma membranes had been permeabilized with digitonin, the responses of the cells to successive pulses of Ca^{2+} in the absence and presence of cyclosporin A were monitored (Fig. 4, and Tables S3 and S4). On average, the ratios of the number of calcium pulses required to induce the PTP in the presence and absence of CsA were similar;

the values were 2.89±0.62 (n=9) in wild-type cells, and 2.48±0.36 (n=4) in HAP1-A12 cells. In HAP1-ΔPPIF cells, which lack cyclophilin D, the value was 0.97±0.07 (n=4) for the clone presented in Fig. 4, and 0.99±0.20 (n=3) for a second clone (data not shown). Thus, in response to pulses of exogenous Ca^{2+}, there was no significant difference in pore opening in the presence and in the absence of subunit c. As expected, disruption of PPIF had removed the sensitivity of the pore to cyclosporin A in HAP1 cells, and, in both wild-type and HAP1-A12 cells, inhibition of the mitochondrial calcium uniporter immediately after a single calcium injection prevented any further uptake of Ca^{2+} by mitochondria (Figs. 5C and F).

Characterization of the vestigial ATP synthase in HAP1-A12 and ρ^0 cells. Despite the significant effect of the removal of subunit c on cellular respiration, the mitochondria of HAP1-A12 cells retain an assembled vestigial ATP synthase complex. This complex, examined by SDS-PAGE analysis (Fig. 5A), and by quantitative mass spectrometry of the subunits of the purified complex (Figs. 5B and S5, and Tables S5 and S6), contained a complete complement of subunits of the F_1-catalytic domain (subunits α, β, γ, δ and ε) and the peripheral stalk (the OSCP, and subunits b, d and F_6. It also retained supernumerary membrane subunits e, f and g, but lacked DAPIT and the mitochondrially encoded subunit ATP6. The analyses suggested also that subunits ATP8 and 6.8PL were absent from the vestigial complex (see Fig. 5A). In contrast, the abundance of one mature form of IF_1, IF_1-M1 (see Fig. S6) found in association with the vestigial complex, had increased by 7-13 fold relative to the wild-type complex**.**

The mitochondria from human 143B ρ^0 cells also retain a vestigial ATP synthase complex resembling the vestigial enzyme complex in HAP1-A12 cells (Figs. 5 and S5, and Tables S7 and S8). It also has a full complement of subunits in the catalytic F_1 and peripheral stalk domains, plus supernumerary subunits e, f and g. The levels of DAPIT and 6.8PL were found to have diminished in mitoplasts relative to wild-type cells (Fig. S5, Table S11), and still more in the purified complex (Fig. S5, Table S7), implying that they are weakly associated

with the complex, and partially lost during its extraction and purification. The relative abundance of the IF_1-M1 form of the inhibitor protein (Fig. S6A) associated with the vestigial complex had increased slightly. However, in ρ^0 cells the mitochondrial import precursor of the inhibitor protein, IF_1-P (see Fig. S6A) was increased by 34-fold relative to parent cells. The presence of IF_1-P in the mitochondria of ρ^0 cells has been noted before (39). These mitochondria also have an active PTP, as reported before (40) and confirmed here, where opening could be stimulated by either ferutinin or thapsigargin and inhibited by cyclosporin A (Fig. S7). Therefore, these experiments with HAP1-A12 and 143B ρ^0 cells together show that subunit c, and also ATP6 and ATP8 are not involved in forming the PTP. An additional more tentative conclusion is that subunits DAPIT and 6.8PL of the ATP synthase are also not part of the PTP.

Oligomeric state of vestigial ATP synthases. The permeability transition pore has been proposed to be associated with dimers, and not monomers of the ATP synthase complex (10, 41). Therefore, the oligomeric state(s) of the vestigial complexes in HAP1-A12 and 143B ρ^0 cells were investigated by extraction of the complexes with digitonin, and native gel electrophoresis of the extract (Fig. 6). Under the conditions employed for the extraction of the complexes from mitoplasts from HAP1-A12 cells for native gel analysis, the vestigial ATP synthase contains two or three related sub-complexes with a smaller apparent molecular weight than the intact monomeric ATP synthase complex (Fig. 6A). Thus, this gel seemed to indicate that the "complex" from HAP1-A12 cells is a mixture of related complexes. This conclusion is not supported by the SILAC data which strongly indicate that it is a single complex (Fig. 5), and that therefore the multiple bands on the native gel are artefactual. It is likely that the removal of the c-ring and accompanying loss of subunits ATP6 and ATP8 destabilises the dimerization interface, which probably relies on subunits e and g, and may also depend on supernumerary subunits f, DAPIT and 6.8PL (17, 18). It is also possible that the vestigial

complex remains dimeric in the membrane and that it is destabilised (monomerised) artefactually by the extraction process. The dependency of the oligomeric state of the ATP synthases and vestigial complexes on conditions for their extraction from mitoplast is illustrated by the analysis of the vestigial complex from 143B ρ^0 cells (Fig. 6B). At the lower concentration of digitonin, the extract contains species corresponding to dimers and monomers of the enzyme, and at the higher concentration of digitonin, monomers and smaller sub-complexes.

Discussion

The experiments described above with HAP1-A12 cells show conclusively by three independent assays of the PTP that, even when the c-protein is absent from their mitochondria, the cells retain a PTP. In intact cells, it opens characteristically in response to treatment with either thapsigargin or ferutinin, and in permeabilized cells in response to elevated concentrations of extramitochondrial Ca^{2+}. In all of these assays, opening of the pore can be inhibited by cyclosporin A. Therefore, the c-ring is not an essential component of the PTP.

Even before these experiments were carried out, a number of features of human c_8-rings were apparent that seemed to be incompatible with the presence in the rings of a non-specific aqueous channel capable of passing hydrophilic molecules with a molecular weight up to 1500 Da (1, 42), as a description of the ring illustrates. The sequence of the identical human and bovine mature c-subunits is 75 amino acids long. In the structure of the bovine c-ring (14), residues 4-37 and 44-74 of each c-subunit are folded into two antiparallel α-helices, arranged respectively in inner and outer rings. The two α-helices in each subunit are joined by extended polar loops from residues 38-43, in the lipid head group region on the matrix side of the inner membrane. Each loop region contains an arginine residue at position 38 and a fully trimethylated lysine residue at position 43 (43). The N-terminal regions extend towards the

space between inner and outer membranes of the organelle, and each has aspartic acid residues at positions 1 and 3, and an unmodified lysine at position 7. Residues in the polar loops and the N-terminal extensions attract cardiolipin molecules selectively over phospholipids (44). With the exception of glutamate-58 on the outer surface of the ring, which plays a central role in the pathway for membrane translocation of protons, the outer surface of the ring is almost entirely hydrophobic, in keeping with its contact with the hydrophobic environment of the inner mitochondrial membrane. The inner surface of the ring is also almost entirely hydrophobic, with the exception of an accessible threonine residue at position 27 (Fig. S8), and it is likely that the central cavity of the mitochondrial c-ring is occupied by lipids, as demonstrated in the related spinach chloroplast c_{14}-rings and the c-ring from *Escherichia coli* (45, 46).

A second structural feature that tends to argue against the c-ring functioning as the PTP is that, in the intact enzyme, access to the central cavity of the c-ring from the matrix side of the membrane is impeded, and possibly completely blocked, by the association of the foot of the central stalk with the c-ring (14) (Fig. S8). At its narrowest point, approximately in the middle of the lipid bilayer, the cavity has a diameter of about 4 Å, widening in both directions to about 12 Å at the external surfaces. The interaction between the c-ring and the central stalk provides a crucial connection between the membrane intrinsic and membrane extrinsic parts of the rotor of the ATP synthase that has to be sufficiently robust to resist the rotational torque of the motor turning at up to 300 Hz. In the structure of the bovine F_1-c_8 complex, the interacting region involves loop regions from five of the c-subunits, and regions of the γ-, δ- and ε-subunits (Fig. S8). The interface is extensive and has a buried surface area of greater than 790 $Å^2$. However, the positions of amino acid side chains in the interface are uncertain, and for that reason they have not been introduced into the structural model. If they were, it is likely that most or all of the small apparent crevice in the interface region leading to the central cavity would be blocked entirely.

One possible way of exposing the central cavity would be to release the central stalk and $\alpha_3\beta_3$-domain, leaving the intact membrane domain with a central cavity freely accessible from both sides of the membrane. In the related V-ATPases, such a physiological mechanism exists as a way of regulating the activity of the enzyme, and a free V_o membrane domain containing the equivalent of the c-ring is produced by the dissociation of the V_1 catalytic domain (47, 48). However, a similar mechanism has not been demonstrated in the mitochondrial F-ATP synthases, and the hydrolytic activity of the enzyme is regulated by a different mechanism involving the inhibitor protein, IF_1 (21). In the purified enzyme and in everted inner membrane vesicles, the interface between the F_1 and membrane domains is resistant to dissociation, for example by mild detergents and mild chaotropes, or by elevated salt concentrations. The only known biochemical way of removing the catalytic domain from membranes so as to leave the membrane domain intact is to dissociate the membrane extrinsic proteins with strong chaotropes such as sodium bromide or guanidinium hydrochloride, leaving the membrane domain of the enzyme intact and protected by the lipid bilayer (49). The only patho-physiological circumstance where isolated human c-rings have been observed is in insoluble storage bodies derived from lysosomes associated with ceroid lipofuschinosis, or Batten's disease (50). Here, the accumulation of c-rings in the storage bodies appears to be derived from defects in a lysosomal pathway for degradation of the c-protein (51).

A somewhat surprising corollary of the demonstration of the PTP in HAP1-A12 cells is that in the absence of subunit c, a vestigial ATPase complex, containing the catalytic and peripheral stalk domains and supernumerary subunits e, f and g, is still assembled in the mitochondria (Fig. 5). However, the vestigial complex and the mitoplasts from which it is derived also lack subunit ATP6. Therefore, neither the proton translocation pathway at the interface of the c-ring and ATP6, nor ATP6 itself, is associated with the PTP. The presence of the PTP in ρ^0 cells, which lack mitochondrial DNA and the encoded ATP6 and ATP8 subunits,

has been noted before (40), and the vestigial F-ATPase complexes from HAP1-A12 cells and 143B ρ^0 cells are remarkably similar, except that the latter contains additionally the c-subunit (presumably organized in the c_8-ring). Thus, the c-ring is not an absolute requirement for the assembly of either the F_1 or peripheral stalk domains.

Both vestigial complexes also probably lack supernumerary subunits DAPIT and 6.8PL, and therefore, they are unlikely to be components of the PTP either. Thus, if the human PTP is associated with the ATP synthase complex, the most likely components available to form the pore are any or all of the remaining membrane subunits, b, e, f and g. If such a pore complex exists, it may not contain any associated F_1 subunits, and so the investigation of the possible involvement of these subunits in pore formation will require the application of specific antibodies and gene disruption approaches to each of the membrane specific subunits of the ATP synthase.

The ATP synthase complex contains a single copy of subunit b with two transmembrane α-helices, and is assumed to contain single copies of subunits e, f and g, each predicted to have a single transmembrane α-helix. Recent cryo-electron microscopy analyses of the ATP synthase complexes suggest that at least subunits e and g are involved in the interface between monomers of the ATP synthase in the dimeric complexes (17, 18). The gene disruption strategy followed for the c-subunit provides a possible approach towards resolving the issue of whether any or all of these subunits are involved in forming the PTP.

Materials and Methods

Cell culture. Near-haploid human HAP1 cells (Horizon Discovery) and derived cell lines HAP1-A12 and HAP1-ΔPPIF (HZGHC004185c012), where the gene encoding cyclophilin D had been disrupted (Horizon Discovery) were grown at 37^{o}C in the presence of 5% carbon dioxide in Iscove's modified Dulbecco's medium (IMDM) plus 10% (v/v) fetal bovine serum

(FBS). Human osteosarcoma 143B cells (ATCC CRL-8303) were grown under similar conditions in Dulbecco's Modified Eagle's Medium (DMEM) containing glucose (4.5 g/L) and pyruvate (110 mg/L), FBS (10%, v/v), penicillin (100 units/mL) and streptomycin (0.1 mg/mL). The medium for cultivation of 143B ρ^0 cells contained additionally uridine (100 μg/mL). To determine cell growth rates, initially, 4 x 10^4 wild-type HAP1 or HAP1-A12 cells were plated in triplicate, and estimates of confluence were made with an IncuCyte HD and 2011A Rev2 software (Essen Bioscience) at 8 h intervals over 4 days.

The oxygen consumption rate (OCR) of cells was determined with a Seahorse XF^e24 instrument (Agilent Technologies). These measurements were made with cells in XF assay medium plus 2 mM glucose and 1 mM pyruvate. 2-Deoxyglucose, oligomycin, carbonyl cyanide-4-(trifluoromethoxy)-phenylhydrazone, and a mixture of rotenone and antimycin A, were introduced successively at final concentrations of 20 mM, 1 μM, 0.5 μM and 0.6 μM each, respectively.

The generation of a mitochondrial membrane potential in wild-type HAP1 cells and HAP1-A12 cells was monitored in digitonin permeabilized cells (see below) by following the fluorescent signal from unbound TMRM (excitation 550 nm/emission 575 nm) with a Shimadzu RF-5301PC spectrofluorophotometer. Permeabilized cells were used at a concentration of 10 x 10^6/ml in 2 ml of a solution containing 120 mM KCl, 10 mM NaCl, 1 mM KH_2PO4, 20 mM MOPS-Tris pH 7.2, and 80 nM TMRM. Fluorescence changes were measured at 30°C with stirring (500 rpm), following the addition of mitochondrial respiratory substrates (5 mM glutamate, 2.5 mM malate, 0.1 mM ADP or 10 mM succinate) and inhibitors (1 μM oligomycin, 1 μM rotenone, 1 μM antimycin-A or 1 μM carbonyl cyanide-4-(trifluoromethoxy)phenylhydrazone) at the times indicated on the traces.

Transcription of the ATP5G1, ATP5G2 and ATP5G3 genes. The levels of transcripts for the c-subunit from ATP5G1, ATP5G2 and ATP5G3 in HAP1 cells relative to β-actin were

estimated by qPCR in an ABI 7900HT Fast Real-Time PCR instrument with specific TaqMan gene expression assays and reagents (Thermo Fisher Scientific).

Disruption of ATP5G1, ATP5G2 and ATP5G3. Three pairs of specific guide RNA molecules (gRNAs) directed against exon IV of genes ATP5G1 and ATP5G2 and exon III of ATP5G3 were identified and optimised with a design tool for CRISPR (clustered regularly interspaced short palindromic repeats; see crispr.mit.edu), synthesised and cloned into the BbsI site of plasmid pSpCas9(BB)-2A-GFP (52) (Addgene). This plasmid encodes the CRISPR associated protein 9 (Cas9) from *Streptococcus pyrogenes* separated from the coding sequence for the green fluorescent protein (GFP) by a 2A sequence. This arrangement leads to GFP being transcribed from the same gene as Cas9, but translated separately from it, allowing cells into which Cas9 has been introduced successfully to be separated and enriched in a fluorescence activated cell sorter. It also expresses the sgRNA consisting of the gRNA fused to a scaffold under the control of the human U6 promoter. The six plasmids (each 0.5 μg) were co-transfected in the presence of lipofectamine 3000 (Thermo Fisher Scientific) into 40-60% confluent HAP1 cells grown in a single well of a six-well plate. Two days later, cells were released with trypsin, and resuspended in IMDM containing 10% (v/v) FBS to a density of 1-2 x 10^6 cells/mL. Green fluorescent cells were separated into single cells in 96 well plates with a High Speed Influx Cell Sorter (BD Biosciences). They were grown at 37^{o}C in the presence of 5% carbon dioxide for 2-3 weeks in IMDM plus 10% FBS until single colonies had formed in each well. Then they were transferred into 24-well plates, expanded in triplicate, and stored at -80^{o}C in IMDM containing 50% (v/v) FBS and 10% (v/v) dimethylsulfoxide.

Cells in a single well were disrupted for 30 min at room temperature with buffer (100 μL) containing 10 mM Tris.Cl, pH 7.4, 0.2% (w/v) SDS, 1x cOmplete EDTA-free proteinase inhibitor cocktail (Roche) and 0.5 units of benzonase (Merck Millipore). Loading buffer (five times normal concentration) was diluted to normal concentration with the sample, and a portion

(10-15 μL) was fractionated on a 10-20% acrylamide gradient protein mini-gel (Thermo Fisher Scientific). Proteins were transferred electrophoretically onto nitrocellulose membranes, and exposed to rabbit antibodies against subunit c (Abcam), and, as loading controls, against Tom20 and the β-subunit of ATP synthase (both Santa Cruz Biotechnology).

The deleted regions of genes were characterized by PCR and DNA sequencing (Source Bioscience). Cells in a single well of a 24-well plate were resuspended in a solution (200 μL) containing 0.2% (w/v) SDS, 75 mM NaCl, 20 mM EDTA and proteinase K (0.4 mg/mL), and the suspension was incubated at 50^{o}C for 2 h. DNA was precipitated with isopropanol, washed with 70% (v/v) ethanol, dried, and redissolved in buffer (100 μL) containing 10 mM Tris.Cl, pH 8.0. The regions containing exons IV of ATP5G1, ATP5G2 and exon III of ATP5G3 were amplified by PCR, and the product sizes analysed by agarose gel electrophoresis. For clone A12, the appropriate PCR fragments were cloned with a TOPO TA Cloning Kit (Thermo Fisher Scientific), and their DNA sequences were determined.

Generation of ρ^0 cells. 143B cells were cultured for ca. 8 weeks as above, but in the presence of ethidium bromide (100 μg/mL) and uridine (100 μg/mL), and then for a further 4-6 passages in the absence of ethidium bromide. The resulting cell line is referred to as 143B-ρ^0. In order to determine that these ρ^0 cells were devoid of mtDNA, total DNA (25 ng) from cells at 90% confluency in a single well was used as a template in real-time PCRs with AmpliTaq Gold DNA polymerase (Applied Biosystems) in an ABI 7900HT Fast Real-Time PCR instrument with primers and probes for the COXII gene in mitochondrial DNA and the nuclear gene for the amyloid precursor protein (53). A 6-carboxyfluorescein fluorophore and a tetramethylrhodamine quencher (Sigma Genosys) were attached to the 5′ and 3′ ends of the probes, respectively. The mtDNA copy number in HAP1-A12 cells was determined by the same method.

Opening of the PTP. The assays were based on the triggering of opening of the pore by three independent methods. In intact human cells pore opening was induced by thapsigargin (4), or ferutinin (5), and, in cells where the plasma membrane had been permeabilized with digitonin, by examination of the capacity of the mitochondria to retain Ca^{2+} introduced exogenously (54).

Assays with thapsigargin and ferutinin. Mitochondrial membrane potential was monitored via the red fluorescence of tetramethylrhodamine methyl ester (TMRM; excitation and emission wavelengths 530 nm and 675 nm, respectively, with a 75 nm span). In order to follow pore opening, cells were loaded with the acetoxymethyl ester of calcein (calcein-AM), which diffuses into the cells and accumulates in cytosolic compartments, including mitochondria. Once inside cells, esterases remove the acetoxymethyl-group to liberate the green fluorescent calcein molecule, which does not cross the mitochondrial or plasma membranes appreciably during the assay. The fluorescence of cytosolic calcein (excitation and emission wavelengths, respectively of 475 and 560 nm, with a 35 nm span) is quenched by $CoCl_2$, which cannot enter mitochondria and so the fluorescence of mitochondrial calcein is maintained. On triggering pore opening with Ca^{2+}, this green fluorescence is quenched (55). In detail, the assay was performed as follows. Cells were grown to 20-30% confluence in 6-well plates. They were washed three times in modified HBSS buffer (1 mL) consisting of Hanks balanced salt solution (containing Ca^{2+} and Mg^{2+}, with no phenol red, Thermo Fisher Scientific) plus 10 mM HEPES, pH 7.4, 2 mM GlutaMAX supplement (Invitrogen) and 1 mM sodium pyruvate, then kept at room temperature for 20 min in modified HBSS (1 mL) containing 1 µM calcein-AM (Life Technologies), 25 nM TMRM, and 8 mM $CoCl_2$ (56). They were washed at 37ºC three times, each for 5 min, with modified HBSS containing 8 mM $CoCl_2$ (1 mL), and incubated at 37ºC in modified HBSS (1 mL) containing 1 mM $CoCl_2$, 20-40 µM thapsigargin or 25 µM ferutinin, for 60 min. When it was employed, the PTP inhibitor CsA (5 µM) was added 5 min before thapsigargin or ferutinin. The concentrations of thapsigargin and CsA were optimised for

HAP1 cells (Figs. S9 and S10). In the optimisation of CsA, cyclosporin H (CsH) was used to determine the extent of any possible off-target impact of cyclosporin compounds. CsH is significantly less effective at inhibiting cyclophilin D than CsA (57). The cells were washed twice with modified HBSS buffer (1 mL) containing 1 mM $CoCl_2$ and finally with phosphate buffered saline (PBS; 2 mL) once. The cells were released from monolayers with trypsin and centrifuged (1300xg, 2 min), and the pellet was resuspended in PBS to a concentration of 1-1.5 x 10^6 cells/mL. Nuclei were stained with Hoechst 33342 dye (10 µg/L, final concentration), and the cell suspension was incubated at 37^{o}C for 15 min. The green and red fluorescence intensities of calcein and TMRM, respectively, in cells with or without treatment with thapsigargin or ferutinin were measured in each individual cell in samples of 5000 cells in a Nucleocounter NC3000 cell counting fluorescence microscope (ChemoMetec). The fluorescence intensities of individual cells were plotted on 2D scatter plots, one with the green and blue and the other with red and blue fluorescence intensities on the ordinate and abscissa, respectively. Orthogonal axes were drawn on the control so as to encompass all of the cells that formed a cluster based on their high fluorescence intensities into the upper two quadrants. The axes were placed automatically in the same positions on the experimental scatter plots, and the percentage fraction of cells in each quadrant was recorded by the instrument (see example in Fig. S11). The ratio of the positive percentage (the sums of "the percentage fractions" in the upper two quadrants) from experimentally perturbed and unperturbed control cells is the "relative ratio". The averages of relative ratios from independent duplicate experiments were plotted on a bar chart. Standard deviations and statistical evaluations by student's t-test were calculated with Excel software.

Capacity of mitochondria to retain calcium. Wild-type HAP1 cells and HAP1-A12 cells were harvested by trypsinization, washed twice in Dulbecco's phosphate buffered saline (DPBS, minus $Ca^{2+}$and Mg^{2+}). They were stained with trypan blue, and counted with a

Countess-II FL automated instrument (Thermo Fisher Scientific). Cells were suspended at a concentration of 20 x 10^6/ml in DPBS containing 2x cOmplete EDTA-free protease inhibitor cocktail (Roche), 20 μM EGTA and digitonin (Calbiochem) to 60 μg/ml, and left on ice for 10 min. The resulting permeabilized cells were washed twice with DPBS containing 1x cOmplete inhibitors. Portions of cells (60 x 10^6) required for individual analyses were centrifuged and the cell pellets were kept on ice. Then a portion of the permeabilized cells was re-suspended at 4ºC in assay buffer (1 ml) containing 20 mM MOPS-Tris pH 7.2, 120 mM KCl, 10 mM NaCl, 1 mM KH_2PO_4, 5 mM glutamate and 2.5 mM malate. The suspension was diluted 3-fold with assay buffer that had been warmed to 30 °C. Calcium green-5N (0.5 μM) and thapsigargin (1 μM), to prevent Ca^{2+} uptake by the endoplasmic reticulum, were added. If it was intended to inhibit the opening of the pore with CsA (1 μM), it was added during this step. After 2 min, successive portions (10 μl) of 3 mM $CaCl_2$ were added (giving a final concentration 10 μM) with stirring (500 rpm), and the fluorescence of the Calcium green-5N (excitation 505 nm, emission 531 nm) was monitored with a Shimadzu RF-5301PC spectrofluorophotometer. The CsA treated and untreated cells were always assessed in immediate succession in order to make them as comparable as possible. The mitochondrial calcium uniporter was inhibited by the addition of 0.5 μM Ru360 (Calbiochem) immediately after a single Ca^{2+} injection.

Purification of ATP synthase. The procedure was carried out at 4ºC. Cells were harvested in PBS containing EDTA-free protease inhibitors (Roche) and total cell protein was estimated by BCA assay (Thermo Scientific). Mitoplasts were prepared by re-suspension of cells to 5 mg/mL in phosphate buffered saline containing 0.5 mg/mL digitonin, 1 mM dithiothreitol and protease inhibitors (58). After 15 min, they were centrifuged (10,500 x g, 5 min), washed in the same solution lacking digitonin, and extracted with buffer A, pH 8.0, containing 0.1 M Tris, 0.15 M NaCl, glycerol (10% v/v), EDTA-free protease inhibitor, 1-palmitoyl-2-oleoyl-sn-glycero-3-phosphocholine (0.09 mg/mL), 1-palmitoyl-2-oleoyl-*sn*-glycero-3-

phosphoethanolamine (0.03 mg/mL), 1-palmitoyl-2-oleoyl-sn-glycero-3-phosphoglycerol (0.03 mg/mL), 2 mM dithiothreitol and digitonin (9 g/g protein). The extract was centrifuged (10,500 x g, 10 min), and the supernatant filtered and stirred for 18 h with an ATP synthase immunocapture resin (Abcam, kit ab109715). The beads were washed in buffer B, differing from buffer A only in the concentration of Tris (20 mM), and the digitonin content (0.05%, w/v). Bound material was eluted in buffer, pH 2.5, containing 0.2 M glycine-HCl and digitonin (0.05%, w/v), and the eluate was neutralised with 1 M Tris.

Mass spectrometric analysis. Stable isotopes were introduced into proteins by stable isotope labelling in cell culture (SILAC). Cells were grown for at least seven doublings in SILAC medium (59) supplemented with proline (200 mg/L), dialysed fetal bovine serum (10%, v/v), penicillin (100 U/mL), streptomycin (100 μg/mL) and either light (R0K0) or heavy (R10K8) isotopes of L-arginine (0.398 mM) and L-lysine (0.798 mM). Each analysis was based on two SILAC experiments one in which the HAP1-A12 cells, or the 143B ρ^0 cells, were labelled in heavy medium and the HAP1 wild-type or the 143B ρ^+ cells in light media, and the second vice versa. Each sample for mass spectrometry consisted of the mitoplast material or ATP synthase purified as above from a 1:1 mixture (based on the protein content) of light and heavy labelled cells (HAP1-A12 and HAP1 wild-type; 143B ρ^0 and 143B ρ^+). Samples were reduced, alkylated and fractionated by SDS-PAGE, and the bands were detected with Coomassie blue dye (60). In-gel tryptic digests (61) of gel slices covering the entire gel track were analysed by LC-MSMS on a Proxeon EASY-nLC system coupled directly to a LTQ OrbiTrap XL or a Q-Exactive Orbitrap mass spectrometer (ThermoFisher Scientific). Data were processed with MaxQuant version 1.5.0.12 and the integrated Andromeda search engine (62, 63), using a Swiss-Prot human protein database (version July 2016) modified to include mature forms of IF_1 with N-terminal residues Phe-25, Gly-26 and Ser-27 (64, 65), and managed further with Perseus (66). Protein ratios for the various forms of IF_1 were calculated from unique peptides

from the import sequence or the N-termini of mature forms, performed manually from the output of the MaxQuant evidence file. The basis of the quantitative experiments using SILAC has been explained before (67).

Acknowledgements. This work was supported by the Medical Research Council, UK by grant MC_U1065663150 and by Programme grant MR/M009858/1, both to J. E. W. H. F. received an MRC PhD studentship.

References

1. Haworth RA, Hunter DR (1979) The Ca^{2+}-induced membrane transition in mitochondria. II. Nature of the Ca^{2+} trigger site. *Arch Biochem Biophys* 195(2):460–467.
2. Zoratti M, Szabò I (1995) The mitochondrial permeability transition. *Biochim Biophys Acta* 1241(2):139–176.
3. Rasola A, Bernardi P (2007) The mitochondrial permeability transition pore and its involvement in cell death and in disease pathogenesis. *Apoptosis* 12(5):815–833.
4. Korge P, Weiss JN (1999) Thapsigargin directly induces the mitochondrial permeability transition. *Eur J Biochem* 265(1):273–280.
5. Abramov AY, Duchen MR (2003) Actions of ionomycin, 4-BrA23187 and a novel electrogenic Ca^{2+} ionophore on mitochondria in intact cells. *Cell Calcium* 33(2):101–112.
6. Crompton M, Ellinger H, Costi A (1988) Inhibition by cyclosporin A of a Ca^{2+}-dependent pore in heart mitochondria activated by inorganic phosphate and oxidative stress. *Biochem J* 255(1):357–360.
7. Elrod JW, Molkentin JD (2013) Physiologic functions of cyclophilin D and the mitochondrial permeability transition pore. *Circ J* 77(5):1111–1122.
8. Kokoszka JE *et al.* (2004) The ADP/ATP translocator is not essential for the mitochondrial permeability transition pore. *Nature* 427(6973):461–465.
9. Baines CP, Kaiser RA, Sheiko T, Craigen WJ, Molkentin JD (2007) Voltage-dependent anion channels are dispensable for mitochondrial-dependent cell death. *Nat Cell Biol* 9(5):550–555.
10. Giorgio V *et al.* (2013) Dimers of mitochondrial ATP synthase form the permeability transition pore. *Proc Natl Acad Sci U S A* 110(15):5887–5892.
11. Walker JE (2013) The ATP synthase: the understood, the uncertain and the unknown.

Biochem Soc Trans 41(1):1–16.

12. Dudkina NV, Heinemeyer J, Keegstra W, Boekema EJ, Braun HP (2005) Structure of dimeric ATP synthase from mitochondria: an angular association of monomers induces the strong curvature of the inner membrane. *FEBS Lett* 579(25):5769–5772.
13. Strauss M, Hofhaus G, Schröder RR, Kühlbrandt W (2008) Dimer ribbons of ATP synthase shape the inner mitochondrial membrane. *EMBO J* 27(7):1154–1160.
14. Watt IN, Montgomery MG, Runswick MJ, Leslie AGW, Walker JE (2010) Bioenergetic cost of making an adenosine triphosphate molecule in animal mitochondria. *Proc Natl Acad Sci U S A* 107(39):16823–16827.
15. Zhou A *et al.* (2015) Structure and conformational states of the bovine mitochondrial ATP synthase by cryo-EM. *Elife* 4:e10180.
16. Morales-Rios E, Montgomery MG, Leslie AGW, Walker JE (2015) Structure of ATP synthase from *Paracoccus denitrificans* determined by X-ray crystallography at 4.0 Å resolution. *Proc Natl Acad Sci U S A* 112(43):13231–13236.
17. Hahn A *et al.* (2016) Structure of a complete ATP synthase dimer reveals the molecular basis of inner mitochondrial membrane morphology. *Mol Cell* 63(3):445–456.
18. Vinothkumar KR, Montgomery MG, Liu S, Walker JE (2016) Structure of the mitochondrial ATP synthase from *Pichia angusta* determined by electron cryo-microscopy. *Proc Natl Acad Sci U S A* 113 (45):12709 –112714.
19. Abrahams JP, Leslie AG, Lutter R, Walker JE (1994) Structure at 2.8 Å resolution of F_1-ATPase from bovine heart mitochondria. *Nature* 370(6491):621–628.
20. Bason JV, Montgomery MG, Leslie AGW, Walker JE (2015) How release of phosphate from mammalian F_1-ATPase generates a rotary substep. *Proc Natl Acad Sci U S A* 112(19):6009–6014.
21. Gledhill JR, Montgomery MG, Leslie AGW, Walker JE (2007) How the regulatory

protein, IF_1, inhibits F_1-ATPase from bovine mitochondria. *Proc Natl Acad Sci U S A* 104(40):15671–15676.

22. Collinson IR *et al.* (1994) ATP synthase from bovine heart mitochondria. *In vitro* assembly of a stalk complex in the presence of F_1-ATPase and in its absence. *J Mol Biol* 242(4):408–421.
23. Dickson VK, Silvester JA, Fearnley IM, Leslie AGW, Walker JE (2006) On the structure of the stator of the mitochondrial ATP synthase. *EMBO J* 25(12):2911–2918.
24. Rees DM, Leslie AGW, Walker JE (2009) The structure of the membrane extrinsic region of bovine ATP synthase. *Proc Natl Acad Sci U S A* 106(51):21597–21601.
25. Fearnley IM, Walker JE (1986) Two overlapping genes in bovine mitochondrial DNA encode membrane components of ATP synthase. *EMBO J* 5(8):2003–2008.
26. Walker JE, Lutter R, Dupuis A, Runswick MJ (1991) Identification of the subunits of F_1F_O-ATPase from bovine heart mitochondria. *Biochemistry* 30(22):5369–5378.
27. Collinson IR *et al.* (1994) F_O membrane domain of ATP synthase from bovine heart mitochondria: purification, subunit composition, and reconstitution with F_1-ATPase. *Biochemistry* 33(25):7971–7978.
28. Chen R, Runswick MJ, Carroll J, Fearnley IM, Walker JE (2007) Association of two proteolipids of unknown function with ATP synthase from bovine heart mitochondria. *FEBS Lett* 581(17):3145–3148.
29. Meyer B, Wittig I, Trifilieff E, Karas M, Schägger H (2007) Identification of two proteins associated with mammalian ATP synthase. *Mol Cell Proteomics* 6(10):1690–1699.
30. Lee J *et al.* (2015) Organization of subunits in the membrane domain of the bovine F-ATPase revealed by covalent cross-linking. *J Biol Chem* 290(21):13308–13320.
31. Dyer MR, Walker JE (1993) Sequences of members of the human gene family for the c subunit of mitochondrial ATP synthase. *Biochem J* 293 (Pt 1):51–64.

32. Yan WL, Lerner TJ, Haines JL, Gusella JF (1994) Sequence analysis and mapping of a novel human mitochondrial ATP synthase subunit 9 cDNA (ATP5G3). *Genomics* 24(2):375–377.

33. Bonora M *et al.* (2013) Role of the c subunit of the F_O ATP synthase in mitochondrial permeability transition. *Cell Cycle* 12(4):674–683.

34. Azarashvili T *et al.* (2014) Potential role of subunit c of F_OF_1-ATPase and subunit c of storage body in the mitochondrial permeability transition. Effect of the phosphorylation status of subunit c on pore opening. *Cell Calcium* 55(2):69–77.

35. Alavian KN *et al.* (2014) An uncoupling channel within the c-subunit ring of the F_1F_O ATP synthase is the mitochondrial permeability transition pore. *Proc Natl Acad Sci U S A* 111(29):10580–10585.

36. Carette JE *et al.* (2011) Ebola virus entry requires the cholesterol transporter Niemann-Pick C1. *Nature* 477(7364):340–343.

37. Essletzbichler P *et al.* (2014) Megabase-scale deletion using CRISPR/Cas9 to generate a fully haploid human cell line. *Genome Res* 24(12):2059–2065.

38. Lieber MR (2010) The mechanism of double-strand DNA break repair by the nonhomologous DNA end-joining pathway. *Annu Rev Biochem* 79:181–211.

39. Wittig I *et al.* (2010) Assembly and oligomerization of human ATP synthase lacking mitochondrial subunits a and A6L. *Biochim Biophys Acta* 1797(6-7):1004–1011.

40. Masgras I, Rasola A, Bernardi P (2012) Induction of the permeability transition pore in cells depleted of mitochondrial DNA. *Biochim Biophys Acta* 1817(10):1860–1866.

41. Carraro M *et al.* (2014) Channel formation by yeast F-ATP synthase and the role of dimerization in the mitochondrial permeability transition. *J Biol Chem* 289(23):15980–15985.

42. Vercesi AE (1984) Dissociation of NAD(P)+-stimulated mitochondrial Ca^{2+}efflux from

swelling and membrane damage. *Arch Biochem Biophys* 232(1):86–91.

43. Walpole TB *et al.* (2015) Conservation of complete trimethylation of lysine-43 in the rotor ring of c-subunits of metazoan adenosine triphosphate (ATP) synthases. *Mol Cell Proteomics* 14(4):828–840.
44. Duncan AL, Robinson AJ, Walker JE (2016) Cardiolipin binds selectively but transiently to conserved lysine residues in the rotor of metazoan ATP synthases. *Proc Natl Acad Sci U S A* 113(31):8687–8692.
45. Oberfeld B, Brunner J, Dimroth P (2006) Phospholipids occupy the internal lumen of the c ring of the ATP synthase of *Escherichia coli*. *Biochemistry* 45(6):1841–1851.
46. Schmidt C *et al.* (2013) Comparative cross-linking and mass spectrometry of an intact F-type ATPase suggest a role for phosphorylation. *Nat Commun* 4:1985.
47. Kane PM (1995) Disassembly and reassembly of the yeast vacuolar H^+-ATPase in vivo. *J Biol Chem* 270(28):17025–17032.
48. Sumner JP *et al.* (1995) Regulation of plasma membrane V-ATPase activity by dissociation of peripheral subunits. *J Biol Chem* 270(10):5649–5653.
49. Collinson IR, Fearnley IM, Skehel JM, Runswick MJ, Walker JE (1994) ATP synthase from bovine heart mitochondria: identification by proteolysis of sites in F_O exposed by removal of F_1 and the oligomycin-sensitivity conferral protein. *Biochem J* 303 (Pt 2):639–645.
50. Palmer DN *et al.* (1992) Mitochondrial ATP synthase subunit c storage in the ceroid-lipofuscinoses (Batten disease). *Am J Med Genet* 42(4):561–567.
51. Ezaki J, Takeda-Ezaki M, Kominami E (2000) Tripeptidyl peptidase I, the late infantile neuronal ceroid lipofuscinosis gene product, initiates the lysosomal degradation of subunit c of ATP synthase. *J Biochem* 128(3):509–516.
52. Ran FA *et al.* (2013) Genome engineering using the CRISPR-Cas9 system. *Nat Protoc*

8(11):2281–2308.

53. He J *et al.* (2012) Human C4orf14 interacts with the mitochondrial nucleoid and is involved in the biogenesis of the small mitochondrial ribosomal subunit. *Nucleic Acids Res* 40(13):6097–6108.

54. Murphy AN, Bredesen DE, Cortopassi G, Wang E, Fiskum G (1996) Bcl-2 potentiates the maximal calcium uptake capacity of neural cell mitochondria. *Proc Natl Acad Sci U S A* 93(18):9893–9898.

55. Petronilli V *et al.* (1999) Transient and long-lasting openings of the mitochondrial permeability transition pore can be monitored directly in intact cells by changes in mitochondrial calcein fluorescence. *Biophys J* 76(2):725–734.

56. Woollacott AJ, Simpson PB (2001) High throughput fluorescence assays for the measurement of mitochondrial activity in intact human neuroblastoma cells. *J Biomol Screen* 6:413–420.

57. Griffiths EJ, Halestrap AP (1991) Further evidence that cyclosporin A protects mitochondria from calcium overload by inhibiting a matrix peptidyl-prolyl cis-trans isomerase. Implications for the immunosuppressive and toxic effects of cyclosporin. *Biochem J* 274 (Pt 2):611–614.

58. Klement P, Nijtmans LG, Van den Bogert C, Houstěk J (1995) Analysis of oxidative phosphorylation complexes in cultured human fibroblasts and amniocytes by blue-native-electrophoresis using mitoplasts isolated with the help of digitonin. *Anal Biochem* 231(1):218–224.

59. Ong SE *et al.* (2002) Stable isotope labeling by amino acids in cell culture, SILAC, as a simple and accurate approach to expression proteomics. *Mol Cell Proteomics* 1(5):376–386.

60. Rhein VF, Carroll J, Ding S, Fearnley IM, Walker JE (2013) NDUFAF7 methylates

arginine 85 in the NDUFS2 subunit of human complex I. *J Biol Chem* 288(46):33016–33026.

61. Wilm M *et al.* (1996) Femtomole sequencing of proteins from polyacrylamide gels by nano-electrospray mass spectrometry. *Nature* 379(6564):466–469.
62. Cox J, Mann M (2008) MaxQuant enables high peptide identification rates, individualized p.p.b.-range mass accuracies and proteome-wide protein quantification. *Nat Biotechnol* 26(12):1367–1372.
63. Cox J *et al.* (2011) Andromeda: a peptide search engine integrated into the MaxQuant environment. *J Proteome Res* 10(4):1794–1805.
64. Xu G, Shin SB, Jaffrey SR (2009) Global profiling of protease cleavage sites by chemoselective labeling of protein N-termini. *Proc Natl Acad Sci U S A* 106(46):19310–19315.
65. Vaca Jacome AS *et al.* (2015) N-terminome analysis of the human mitochondrial proteome. *Proteomics* 15(14):2519–2524.
66. Tyanova S *et al.* (2016) The Perseus computational platform for comprehensive analysis of (prote)omics data. *Nat Methods* 13(9):731–740.
67. Cox J, Mann M (2011) Quantitative, high-resolution proteomics for data-driven systems biology. *Annu Rev Biochem* 80:273–299.

Figures

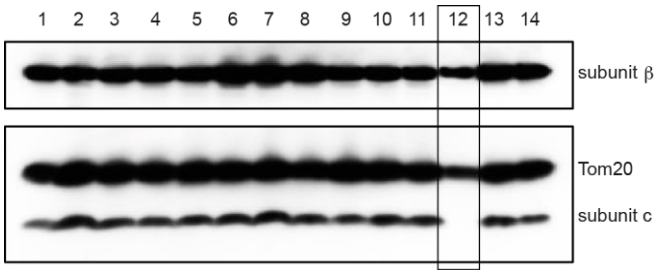

Fig. 1. Expression of the c-subunit of human ATP synthase in HAP1 clonal cells following attempted disruption of genes ATP5G1, ATP5G2 and ATP5G3. Total cell proteins from each clone were fractionated by SDS-PAGE, and the β- and c-subunits of the ATP synthase and Tom20 were detected with antibodies. The results for 14 of the 24 clones that were examined are shown. The A12 clone lacking subunit c is boxed. The signals from the β-subunit and Tom20 are weaker than in other tracks because the HAP1-A12 clone grows slower, and thus the analysed colony contains fewer cells.

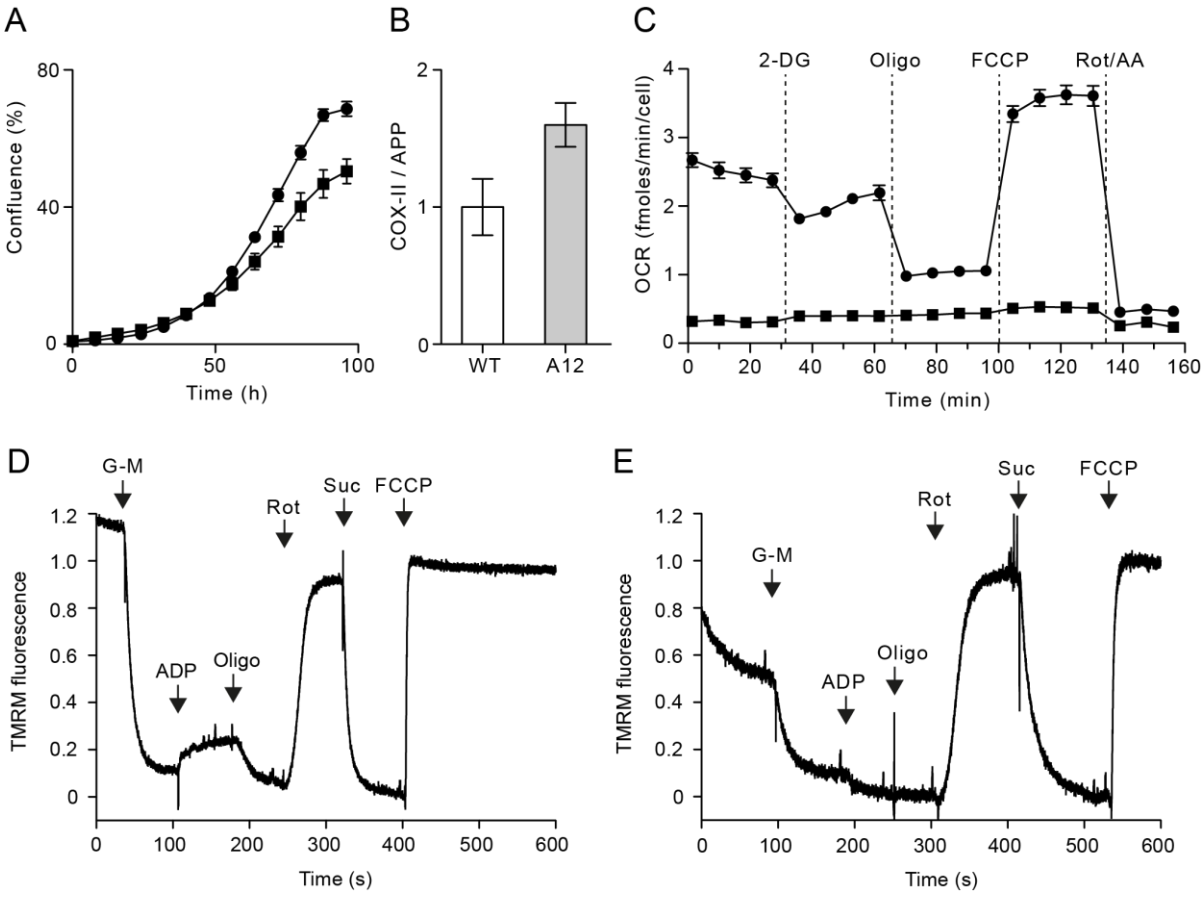

Fig. 2. Characteristics of HAP1-A12 cells. In A and C, ●, HAP1 wild-type cells; ■, HAP1-A12 cells. A, growth rates of HAP1 cells. About 40,000 cells were seeded into individual wells of a 6-well plate, and their confluence was monitored over 96 h. The data points are the mean values ±SD (n=3); B, the relative copy numbers of mtDNA in HAP1 cells. Regions of the genes for COX II and the amyloid precursor protein (APP) were amplified and quantitated as indices of mitochondrial and nuclear DNA, respectively. All data are the mean values ±SDs (n=4); C, cellular oxygen consumption rates (OCR) before and after sequential additions of 2-deoxyglucose (2-DG), oligomycin (Oligo), carbonyl cyanide-4-(trifluoromethoxy)phenylhydrazone (FCCP), and a mixture of rotenone and antimycin A (Rot/AA), at the times indicated. Data represent the mean ±SEM (n=8 or 9 wells). D and E, TMRM fluorescence measurements with permeabilized wild-type HAP1 and HAP1-A12 cells, respectively, normalized to zero after the addition of succinate and to 1 following FCCP treatment; 5 mM glutamate and 2.5 mM malate (G-M), 0.1 mM ADP; 1 μM oligomycin (Oligo), 1 μM rotenone (Rot), 10 mM succinate (Suc), and 1 μM FCCP were added as indicated.

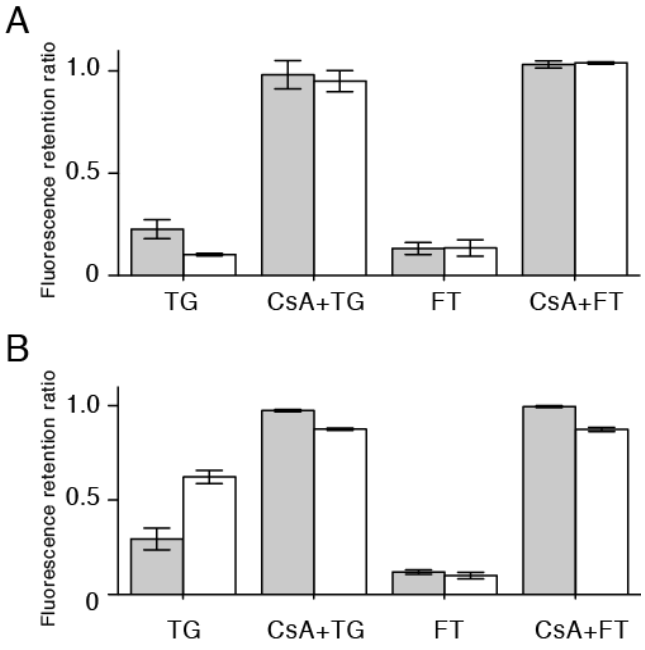

Fig. 3. The opening of the PTP in HAP1 cells. A, wild-type cells; B, HAP1-A12 cells. The cells were stained with both calcein and TMRM, and then incubated for 1 h in the presence of either 40 μM thapsigargin (TG) or 25 μM ferutinin (FT). Duplicate samples were incubated first in the presence of 5 μM cyclosporin A (CsA), and then treated with either thapsigargin or ferutinin. Grey and white columns correspond to the retention ratios for calcein and TMRM, respectively, compared with cells treated with the vehicle DMSO only. All data are mean values ±SDs (n=4).

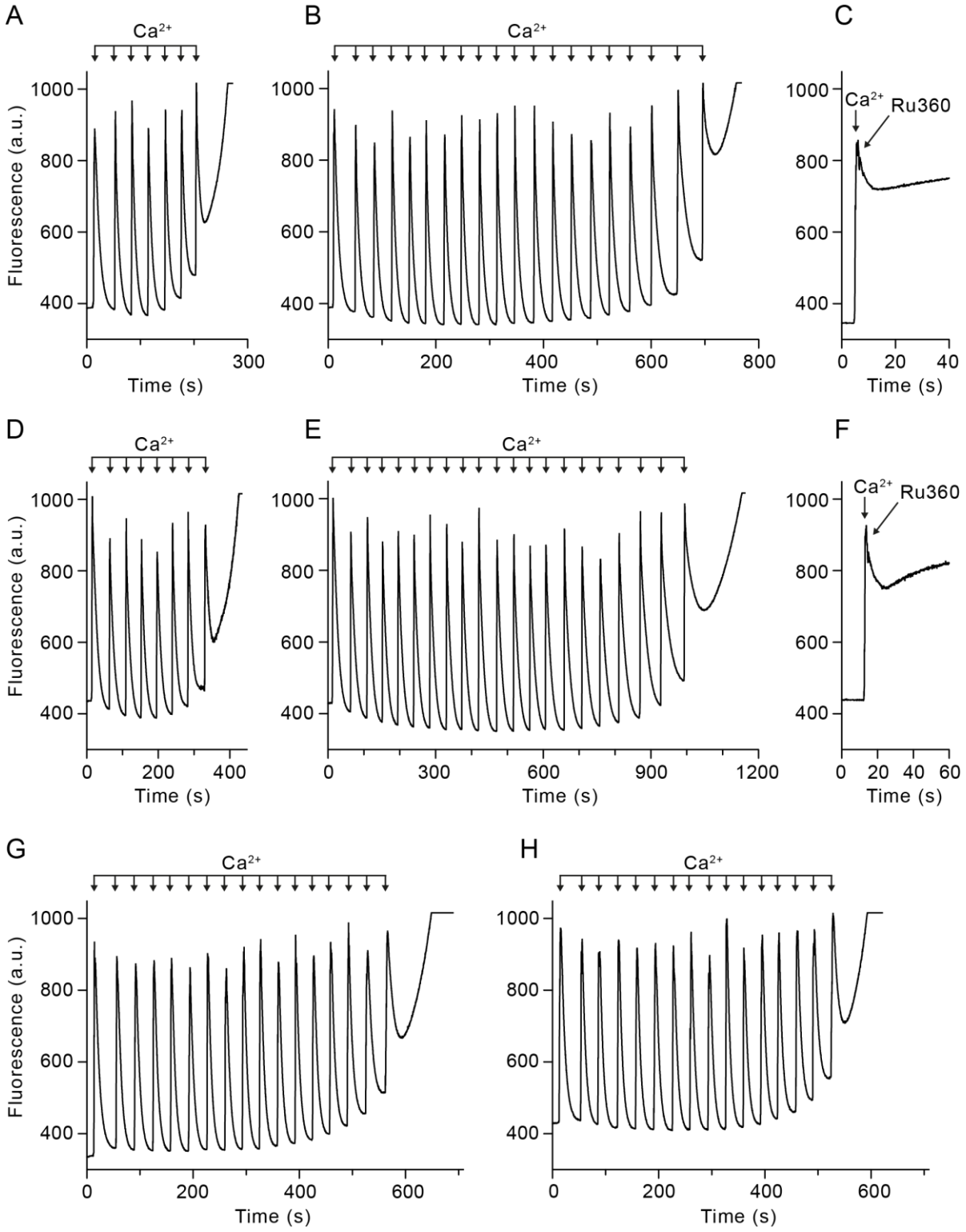

Fig. 4. Calcium induced opening of the PTP in permeabilized HAP1 cells. A-C, wild-type cells; D-F, HAP1-A12 cells; G-H, HAP1-ΔPPIF cells. The calcium retention capacity of mitochondria in digitonin permeabilized cells (20 x 10^6 cells/ml) was examined in response to pulses of 10 μM $CaCl_2$. Extra-mitochondrial Ca^{2+} was measured with Calcium green-5N

fluorescence (a.u., arbitrary unit). A, D and G, and B, E and H, respectively, the calcium retention capacity in the absence and presence of CsA (1 μM). C and F, effect on wild-type and HAP1-A12 cells, respectively, of inhibition of the mitochondrial calcium uniporter with Ru360 (0.5 μM) added immediately after a single pulse of Ca^{2+}.

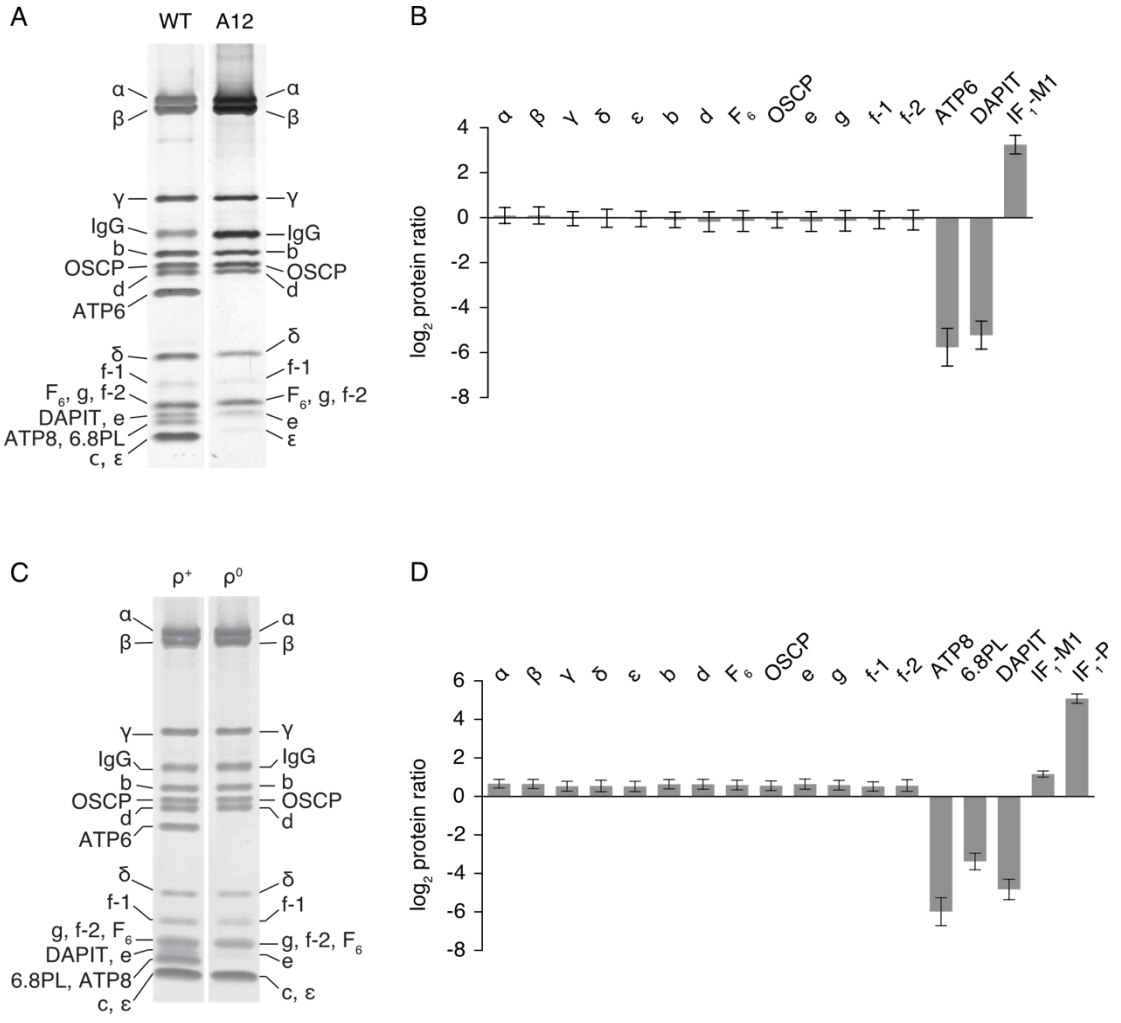

Fig 5. Effects of the deletion of the c-subunit of human ATP synthase in HAP1-A12 cells, and of the removal of ATP6 and ATP8 in ρ^0 cells. Part A, impact of removal of c-subunits on the subunit composition of the vestigial ATP synthase complex. The complex was purified from mitoplasts derived from wild-type (WT) HAP1 and HAP1-A12 cells and analyzed by SDS-PAGE. Part B, relative abundance of subunits of ATP synthase and one of the mature forms of the ATPase inhibitor protein, IF_1-M1 (see Fig. S6). The complex and residual complex were

purified from a 1:1 mixture of SILAC-labelled wild-type HAP1 cells and HAP1-A12 cells, respectively, and tryptic peptides were analyzed by quantitative mass spectrometry. The experiment was performed twice with reciprocal protein labelling. The bars represent median values of both relative abundance ratios determined for proteins identified in the complementary SILAC labelling experiments. Error bars show the range of the two values. Parts C and D, ATP synthase and the vestigial complex purified by immunocapture from digitonin extracts of mitoplasts from 143B ρ^+ and ρ^0 cells and analyzed as in A and B respectively. The proteins in A and C were stained with silver. Subunits were identified by mass spectrometric analysis of tryptic digests of bands from a duplicate gel stained with Coomassie blue dye. The histograms are derived from the data in Fig. S5 and Tables S5-S8. Isoforms 1 and 2 of the f-subunit (f-1 and f-2; see Fig. S6) were identified in human cells.

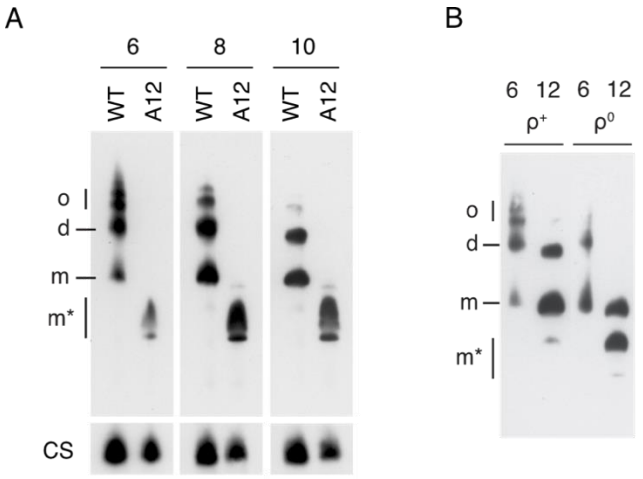

Fig. 6. Oligomeric state of ATP synthase in HAP1 and 143B ρ^+ cells, and of vestigial ATP synthase complexes in HAP1-A12 and 143B ρ^0 cells. Mitoplasts were extracted with various concentrations of digitonin/protein (w/w) indicated above each lane. The ATP synthase and vestigial complexes were purified by immunoaffinity, and analysed by BN-PAGE and detected by Western blotting with an antibody against the β-subunit. Parts A and B, analysis of, respectively, HAP1 wild-type (WT) and HAP1-A12 cells, and 143B ρ^+ and ρ^0 cells. In A,

citrate synthase (CS) was employed as a loading control. o, oligomers; d, dimers; m, monomers; m*, other complexes of unknown oligomeric state.

Supplementary information for:

Persistence of the mitochondrial permeability transition in the absence of subunit c of human ATP synthase

Jiuya He, Holly C. Ford, Joe Carroll, Shujing Ding, Ian M. Fearnley and John E. Walker

The Medical Research Council Mitochondrial Biology Unit, Cambridge Biomedical Campus, Hills Road, Cambridge CB2 0XY, United Kingdom

A

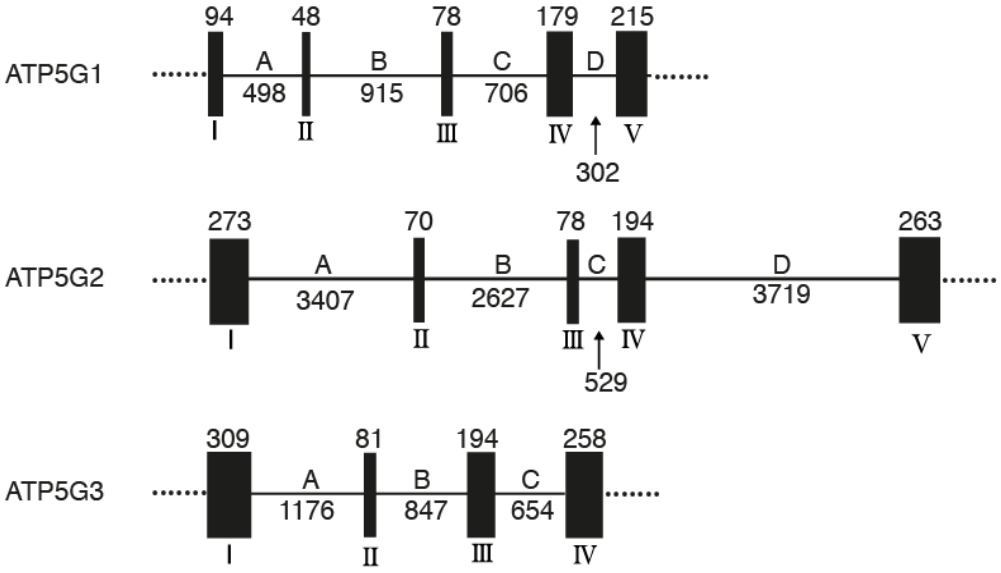

B

```
ATP5G1 MQTAGALFISPALIRCCTRGLIRPVSASFLNSPVNSSKQPSY------SNFPLQVARREF 54
ATP5G2 MFACSKFVSTPSLVKSTSQLLSRPLSAVVLKRPEILTDESLSSL-AVSCPLTSLVSSRSF 59
ATP5G3 MFACAKLACTPSLIRAGSRVAYRPISASVLSRPEASRTGEGSTVFNGAQNGVSQLIQREF 60
       * :.. :  :*:*::. ::   **:** .*. *                  :  *.*

ATP5G1 QTSVVSRDIDTAAKFIGAGAATVGVAGSGAGIGTVFGSLIIGYARNPSLKQQLFSYAILG 114
ATP5G2 QTSAISRDIDTAAKFIGAGAATVGVAGSGAGIGTVFGSLIIGYARNPSLKQQLFSYAILG 119
ATP5G3 QTSAISRDIDTAAKFIGAGAATVGVAGSGAGIGTVFGSLIIGYARNPSLKQQLFSYAILG 120
       ***.:************************************************************

ATP5G1 FALSEAMGLFCLMVAFLILFAM 136
ATP5G2 FALSEAMGLFCLMVAFLILFAM 141
ATP5G3 FALSEAMGLFCLMVAFLILFAM 142
       **********************
```

Fig. S1. Structures of the human ATP5G1, ATP5G2 and ATP5G3 genes and the sequences of the three encoded precursors of the c-subunit of the ATP synthase. A, the genes; exons I-V and introns A-D are represented by solid boxes and continuous lines, respectively. Their sizes are given in base pairs. B, the sequences of the encoded proteins. Only the import sequences are surrounded by blue. Asterisks denote identities.

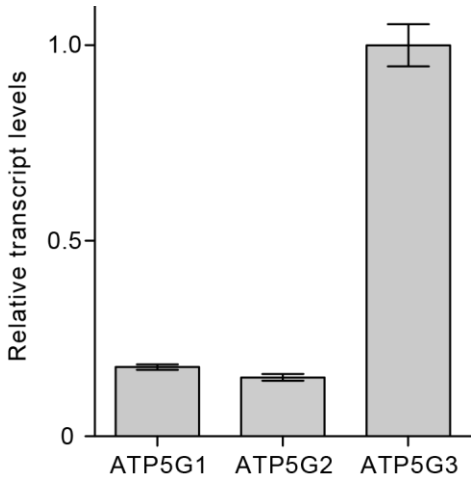

Fig. S2. Transcription of the human genes ATP5G1, ATP5G2 and ATP5G3 in HAP1 cells. The values are normalized to endogenous β-actin and displayed relative to the ATP5G3 transcript, and the error bars show the standard deviations.

Table S1. Target site for gRNA molecules employed in the disruption of the human ATP5G1, ATP5G2 and ATP5G3 genes.

gRNA	Target site
ATP5G1-1	ACAGCAACTTCCCACTCCAG
ATP5G1-2	TGTTTGGCAGCTTGATCATT
ATP5G2-1	GCGCCATTTCAAGGGACATC
ATP5G2-2	CTGGGATTGGAACTGTGTTT
ATP5G3-1	AAGGGAGTTTCAGACCAGTG
ATP5G3-2	GCTGCCAAATTTATTGGTGC

Table S2. Primers employed in the amplification by PCR of the exon targeted by gRNAs in the human ATP5G1, ATP5G2 and ATP5G3 genes.

Primer	Sequence
ATP5G1-Forward	GCAGTTTGCCAACAGTTTCAGAG
ATP5G1-Reverse	GATGAAATCAACCTGAAGGCTCCTG
ATP5G2-Forward	AGGCAAATGCTTCTGAGGCT
ATP5G2-Reverse	GTGCCAGTTTTCCCAGGAGT
ATP5G3-Forward	ATTTGTCTCTTTACACTCAGCTACA
ATP5G3-Reverse	GCTAAGTTTCCAACTACTGCAAGC

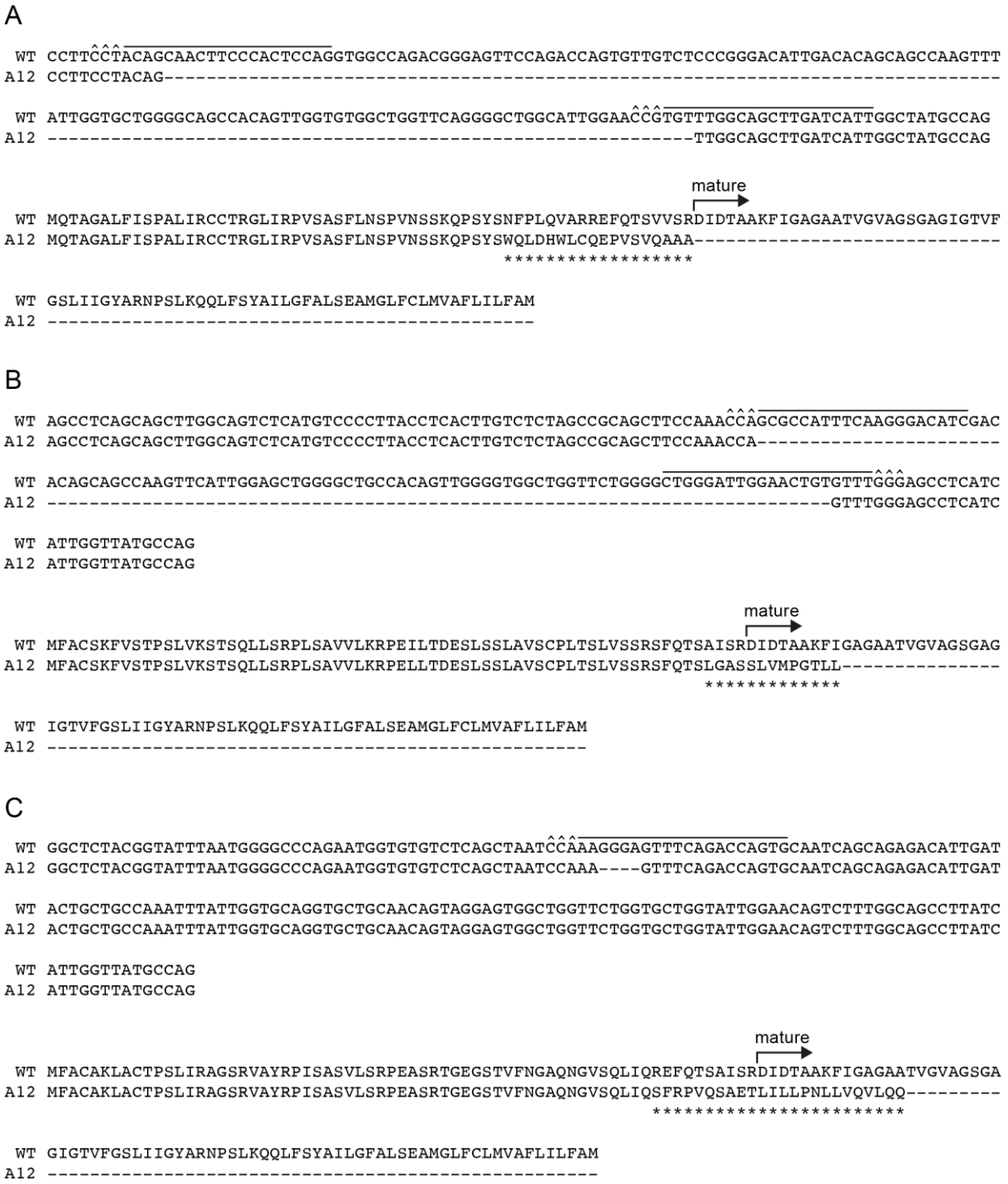

Fig. S3. Deletion of sequences in HAP1 wild-type cells to produce the HAP1-A12 strain. In A-C are shown exons IV of the human ATP5G1 and ATP5G2, and exon III of the ATP5G3 gene, respectively, encoding the subunit c of human ATP synthase. In the upper part of each panel, the sequences of the targeted exon of each gene in the parental or wild-type (WT) cells are aligned with the corresponding deleted sequence in the HAP1-A12 cells. Carets indicate

the PAM (protospacer adjacent motif) sequences for each guide RNA, and solid bars the guide RNA target sequences. In the lower part of A-C, the impacts of the deletions on the sequences of the import precursors of the c-subunit are shown. The start of the mature protein is indicated. Amino acid changes introduced by the process of deletion are indicated by asterisks. Dashed lines indicate deletions in DNA and protein sequences.

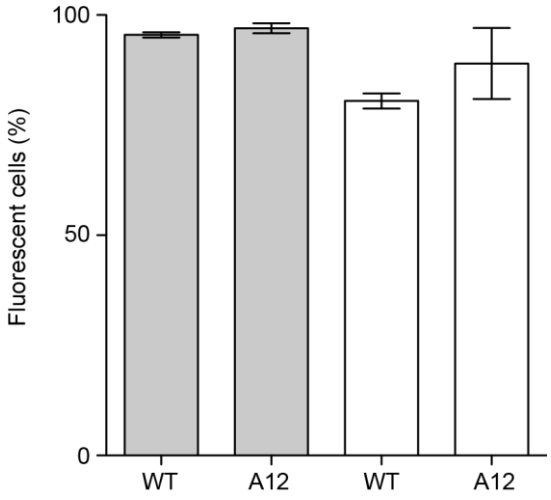

Fig. S4. Comparison of the efficiency of staining of HAP1 wild-type cells and HAP1-A12 cells by calcein and TMRM. Grey and white histograms correspond to cells stained with calcein and/or TMRM, respectively. The percentage of fluorescent cells was determined with a Nucleocounter 3000. All data are the mean values ± SDs (n=4).

Table S3. Number of calcium pulses recorded in permeabilized wild-type HAP1 cells.

The values in the first row refer to Fig. 4A and 4B. Rows 2-9 correspond to replicate experiments.

No CsA	With CsA	Ratio
7	20	2.86
6	26	4.33
5	13	2.6

11	25	2.27
7	21	3.0
11	30	2.86
7	21	3.0
7	21	3.0
5	11	2.2
Av. 7.3	Av. 20.9	Av. 2.89
SD. 2.2	SD. 6.0	SD. 0.62

Table S4. Number of calcium pulses recorded in permeabilized HAP1-A12 cells.

The values in the first row refer to Fig. 4D and 4E. Rows 2-4 correspond to replicate experiments.

No CsA	With CsA	Ratio
8	21	2.63
14	40	2.86
9	18	2.0
7	17	2.43
Av. 9.5	Av. 24.0	Av. 2.48
SD. 3.1	SD. 10.8	SD. 0.36

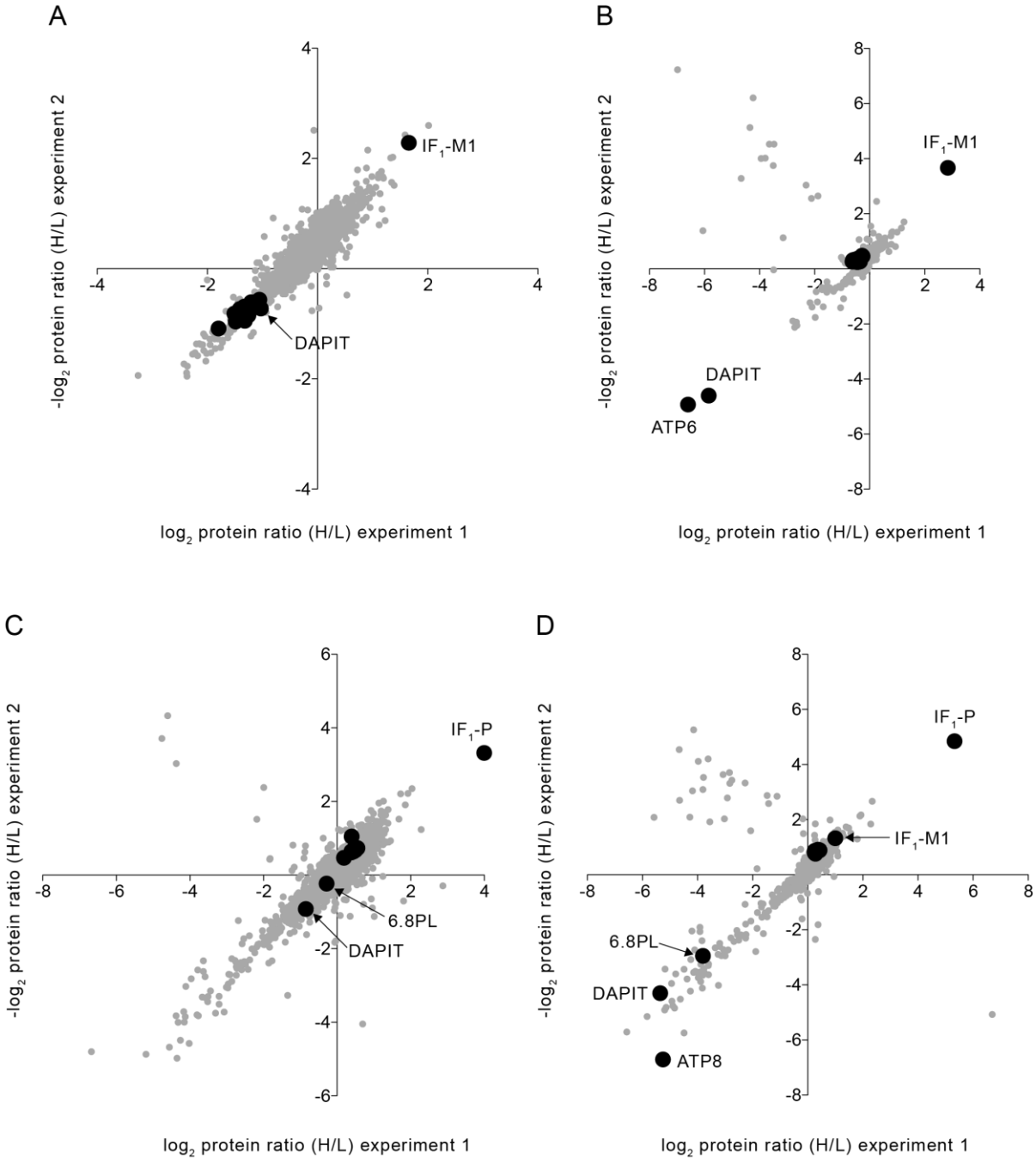

Fig. S5. Effects on protein relative abundance of the deletion of the c-subunit of human ATP synthase in HAP1 cells, and of the removal of ATP6 and ATP8 in 143B ρ^0 cells. Relative quantitative mass spectrometry analyses of proteins in mitoplasts (parts A and C) and purified ATP synthase (parts B and D) prepared from a 1:1 mixture of cells that were differentially SILAC-labelled. Panels A and B show the analyses of wild-type HAP1 cells combined with HAP1-A12 cells devoid of the ATP synthase c-subunit, and C and D the data from wild-type

143B ρ^+ cells and ρ^0 cells lacking mitochondrial DNA. The experiments were performed twice, using reciprocal SILAC labelling orientations. For all the scatter plots each data point corresponds to the relative abundance ratio of an identified protein from the two complementary labelling experiments. ●, ATP synthase subunits and the precursor (P), or the M1 mature form of IF_1; ●, all other identified proteins. Protein ratios and peptide evidence for IF_1 are listed in Tables S5 to S12.

A

```
          *       10          20          30          40          50          60
IF1-P     MAVTALAARTWLGVWGVRTMQARGFGSDQSENVDRGAGSIREAGGAFGKREQAEEERYFR
IF1-M1                              FGSDQSENVDRGAGSIREAGGAFGKREQAEEERYFR
IF1-M2                               GSDQSENVDRGAGSIREAGGAFGKREQAEEERYFR
```

B

```
          *       10          20          30          40          50          60
f-1   MASVGECPAPVPVKDKKLLEVKLGELPSWILMRDFSPSGIFGAFQRGYYRYYNKYINVKK
f-2   MASV------VPVKDKKLLEVKLGELPSWILMRDFSPSGIFGAFQRGYYRYYNKYINVKK

                  70          80          90
f-1   GSISGITMVLACYVLFSYSFSYKHLKHERLRKYH
f-2   GSISGITMVLACYVLFSYSFSYKHLKHERLRKYH
```

Fig. S6. Sequences of the precursor and mature forms of the inhibitor protein IF_1 and isoforms of subunit f of the human mitochondrial ATP synthase. The asterisks denote that the initiator methionine residue has been removed, and residue alanine-2 has been Nα-acetylated. A, residues 1-60 of the initial precursor form of IF_1 (top line) and formation of IF_1-P, and below the observed mature forms IF_1-M1 and IF_1-M2; B, complete sequences of isoforms f-1 and f-2. They arise by an alternative splicing mechanism, and differ in the region denoted by shading and dashes. Both isoforms were observed in mass spectrometric analyses. Subunit f lacks a processed N-terminal mitochondrial import sequence.

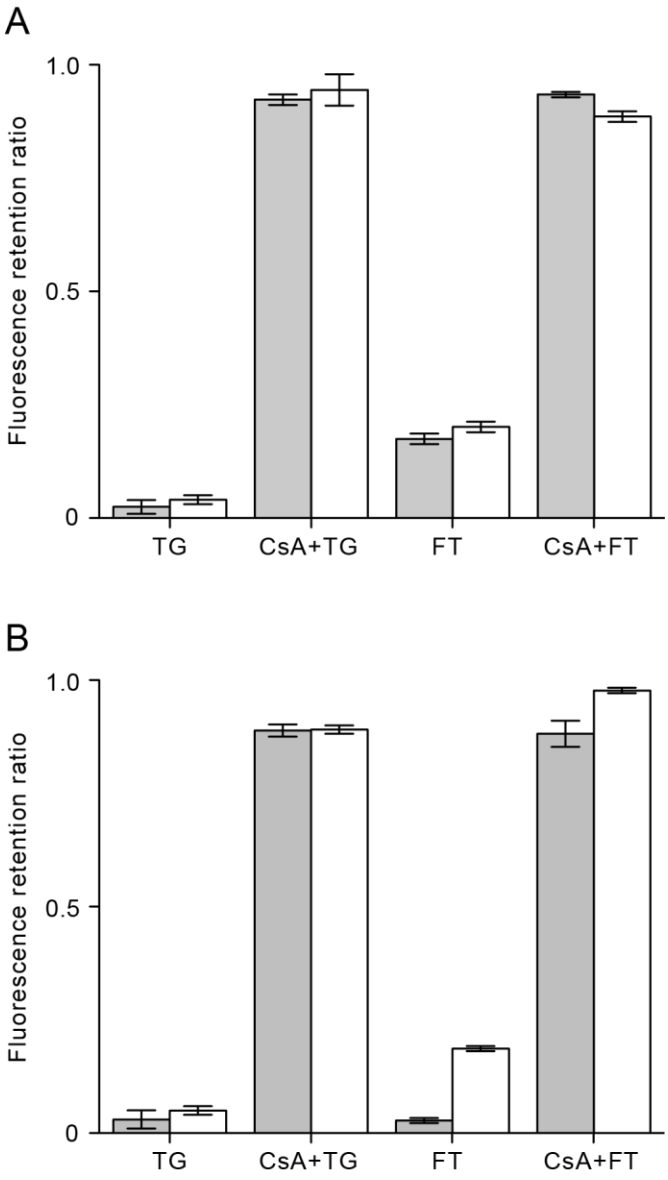

Fig. S7. Presence of the PTP in human 143B cells. A, and B, ρ^+ and ρ^0 cells. Retention ratios in 143B cells for calcein (grey) and TMRM (white). The cells were treated with 20 μM thapsigargin (TG) or 25 μM ferutinin (FT) for 1 h, respectively, with or without CsA (5 μM). TG activated cells were treated with CsA before staining whereas the FT cells were stained with calcein and TMRM, and then treated with CsA. All ratios were normalized to the untreated 143B cells (loaded with DMSO vehicle). The data represent means ± SDs (TG, n=4; FT, n=2).

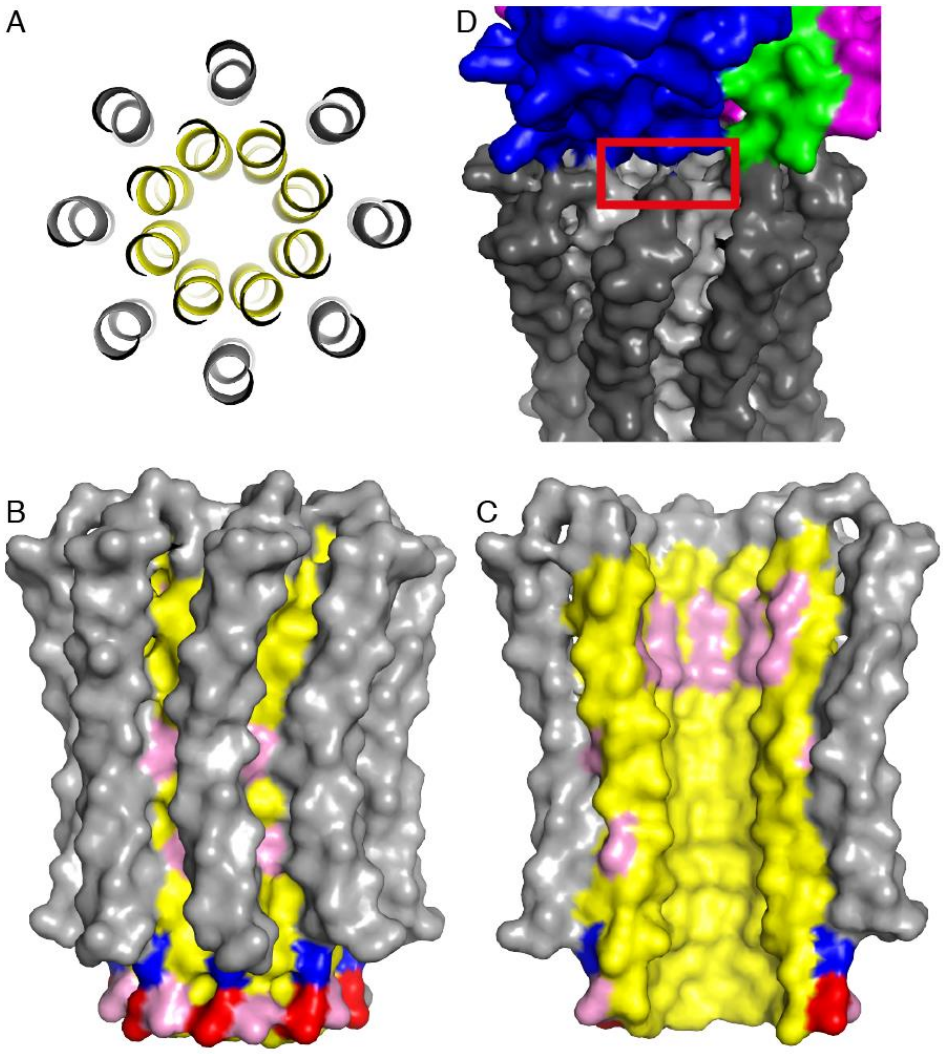

Fig. S8. Structure of the c_8-ring from bovine ATP synthase. As the sequences of the bovine and human c-subunits are the same, the structures of their c_8-rings are identical. A, cross-section of the ring showing concentric annuli of N- and C-terminal transmembrane α-helices; B, external view of the surface of the intact ring (inner and outer yellow and grey rings, respectively); C, internal view of the surface of half of the ring (four c-subunits). In the inner ring, yellow, pink, red and blue regions denote hydrophobic, hydrophilic, basic and acidic residues, respectively; D, view of the region of contact between the c_8-ring (below) and foot of the central stalk, in the enzyme's rotor. Blue, green and magenta areas are parts of the γ-, δ- and ε-subunits. The c_8-ring is grey. The red box indicates a small crevice in the model at 3.5 Å

resolution leading to the central cavity. In reality, the crevice is probably occupied by the side chains of amino acids, which were truncated at the β-carbon atom in the model.

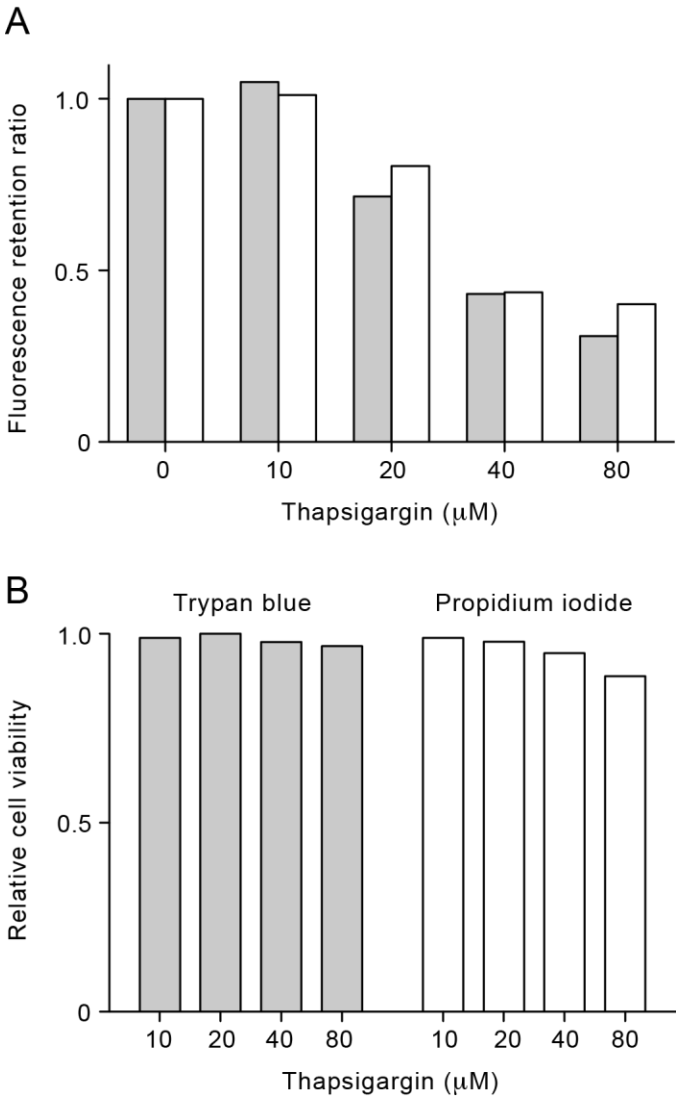

Fig. S9. Optimisation of thapsigargin concentrations on the opening of the PTP in wild-type HAP1 cells. A, the cells were stained with both calcein and TMRM, then incubated for 1 h with various concentrations of thapsigargin. Grey and white columns represent the retention ratios for calcein and TMRM fluorescence signals, respectively, relative to untreated cells. B, HAP1 cell viability after treatment with thapsigargin for 1 h was assessed by both trypan blue and propidium iodide staining, with a Countess-II FL automated cell counter (Thermo Fisher Scientific) or a NC3000 advanced image cytometer (ChemoMetec), respectively. The values

are expressed relative to untreated HAP1 cells.

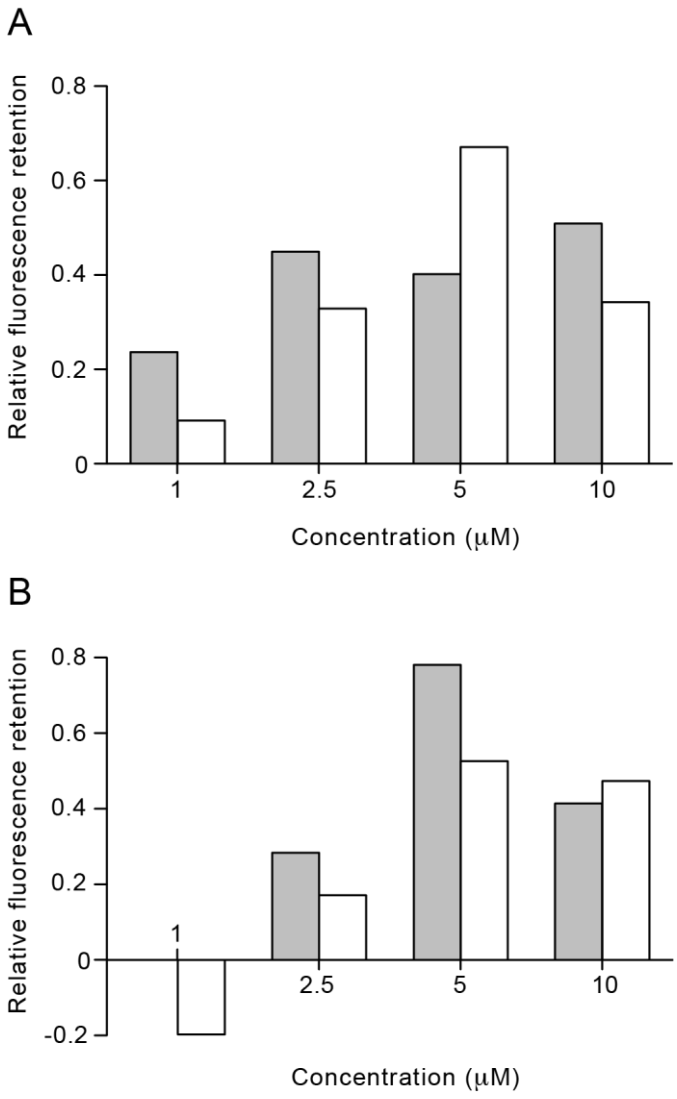

Fig. S10. Cyclosporin A concentration dependent inhibition of the PTP in wild-type HAP1 cells. Cells were stained with both calcein and TMRM, then pre-incubated with different concentrations of CsA or CsH for 5 min, and then treated for 1 h with 40 μM thapsigargin (A) or 25 μM ferutinin (B). The fluorescence retention ratio for calcein and TMRM was determined, relative to untreated cells. Grey and white columns difference values (CsA minus CsH) for calcein and TMRM fluorescence signals, respectively.

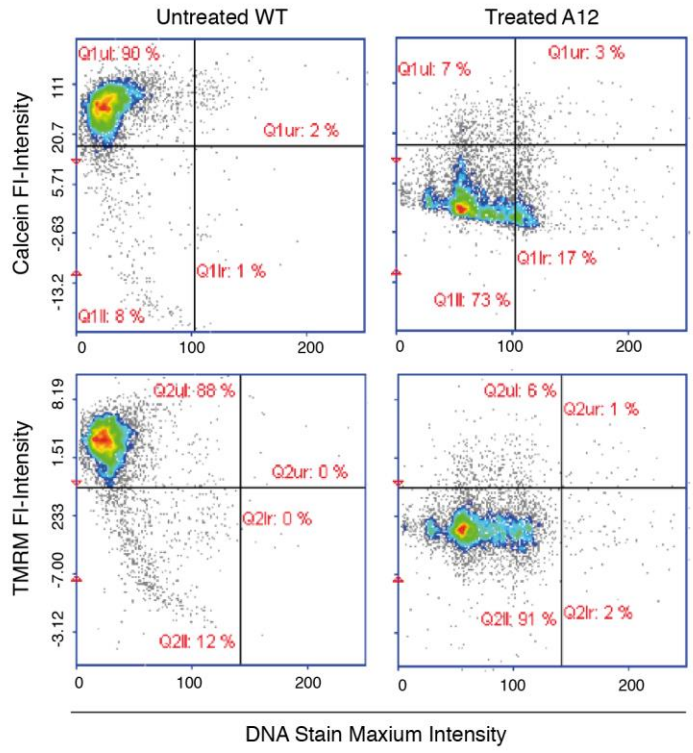

Fig. S11. An example of scatter plots used in the assay of the PTP. HAP1-A12 (A12) and HAP1 wild-type (WT) cells were stained with both calcein and TMRM. Then both sets of cells were incubated for 1 h in the presence of 25 μM ferutinin (FT) or DMSO vehicle, respectively. Green and red fluorescence intensities of calcein and TMRM, respectively, of samples of 5000 cells with or without treatment with ferutinin were measured in a Nucleocounter NC3000 cell counting fluorescence microscope (ChemoMetec). Then, orthogonal axes were drawn manually on the 2D scatter plots for the WT cells and then used as the master template for the scatter plots for the HAP1-A12 cells. The relative calcein retention ratio was calculated as the ratio of HAP1-A12 positive percentages (the sum of the two percentages in the upper quadrants for A12: 7+3%=10%) and the positive percentages for wild-type cells (WT) (the sum of the two percentages in the corresponding upper quadrants: 90+2%=92%). The values of intensities on both axes should be multiplied by 10^3.

Supplementary Table S5. Proteins identified in SILAC experiments comparing immunopurifed ATP synthase from wild-type and HAP1-A12 cells.

Supplementary Table S6. Peptide data for the ATPase inhibitor protein obtained in SILAC experiments comparing ATP synthase from wild-type and HAP1-A12 cells.

Supplementary Table S7. Proteins identified in SILAC experiments comparing immunopurified ATP synthase from wild-type and 143B ρ^0 cells.

Supplementary Table S8. Peptide data for the ATPase inhibitor protein obtained in SILAC experiments comparing ATP synthase from wild-type and ρ^0 143B cells.

Supplementary Table S9. Proteins identified in SILAC experiments comparing mitoplasts from wild-type and HAP1-A12 cells.

Supplementary Table S10. Peptide data for the ATPase inhibitor protein obtained in SILAC experiments comparing mitoplasts from wild-type and HAP1-A12 cells.

Supplementary Table S11. Proteins identified in SILAC experiments comparing mitoplast material from wild-type and 143B ρ^0 cells.

Supplementary Table S12. Peptide data for the ATPase inhibitor protein obtained in SILAC experiments comparing mitoplasts from wild-type and 143B ρ^0 cells.

Supplementary information for:

Persistence of the mitochondrial permeability transition in the absence of subunit c of human ATP synthase

Jiuya He, Holly C. Ford, Joe Carroll, Shujing Ding, Ian M. Fearnley and John E. Walker

The Medical Research Council Mitochondrial Biology Unit, Cambridge Biomedical Campus, Hills Road, Cambridge CB2 0XY, United Kingdom

Materials and Methods

Cell culture. Near-haploid human HAP1 cells (Horizon Discovery) and derived cell lines HAP1-A12 and HAP1-ΔPPIF (HZGHC004185c012), where the gene encoding cyclophilin D had been disrupted (Horizon Discovery) were grown at 37^{o}C in the presence of 5% carbon dioxide in Iscove's modified Dulbecco's medium (IMDM) plus 10% (v/v) fetal bovine serum (FBS). Human osteosarcoma 143B cells (ATCC CRL-8303) were grown under similar conditions in Dulbecco's Modified Eagle's Medium (DMEM) containing glucose (4.5 g/L) and pyruvate (110 mg/L), FBS (10%, v/v), penicillin (100 units/mL) and streptomycin (0.1 mg/mL). The medium for cultivation of 143B ρ^0 cells contained additionally uridine (100 μg/mL). To determine cell growth rates, initially, 4 x 10^4 wild-type HAP1 or HAP1-A12 cells were plated in triplicate, and estimates of confluence were made with an IncuCyte HD and 2011A Rev2 software (Essen Bioscience) at 8 h intervals over 4 days.

The oxygen consumption rate (OCR) of cells was determined with a Seahorse XF^{e}24 instrument (Agilent Technologies). These measurements were made with cells in XF assay medium plus 2 mM glucose and 1 mM pyruvate. 2-Deoxyglucose, oligomycin, carbonyl cyanide-4-(trifluoromethoxy)-phenylhydrazone, and a mixture of rotenone and antimycin A, were introduced successively at final concentrations of 20 mM, 1 μM, 0.5 μM and 0.6 μM each, respectively.

The generation of a mitochondrial membrane potential in wild-type HAP1 cells and HAP1-A12 cells was monitored in digitonin permeabilized cells (see below) by following the fluorescent signal from unbound TMRM (excitation 550 nm/emission 575 nm) with a Shimadzu RF-5301PC spectrofluorophotometer. Permeabilized cells were used at a concentration of 10 x 10^6/ml in 2 ml of a solution containing 120 mM KCl, 10 mM NaCl, 1 mM KH_2PO4, 20 mM MOPS-Tris pH 7.2, and 80 nM TMRM. Fluorescence changes were

measured at 30°C with stirring (500 rpm), following the addition of mitochondrial respiratory substrates (5 mM glutamate, 2.5 mM malate, 0.1 mM ADP or 10 mM succinate) and inhibitors (1 μM oligomycin, 1 μM rotenone, 1 μM antimycin-A or 1 μM carbonyl cyanide-4-(trifluoromethoxy)phenylhydrazone) at the times indicated on the traces.

Transcription of the ATP5G1, ATP5G2 and ATP5G3 genes. The levels of transcripts for the c-subunit from ATP5G1, ATP5G2 and ATP5G3 in HAP1 cells relative to β-actin were estimated by qPCR in an ABI 7900HT Fast Real-Time PCR instrument with specific TaqMan gene expression assays and reagents (Thermo Fisher Scientific).

Disruption of ATP5G1, ATP5G2 and ATP5G3. Three pairs of specific guide RNA molecules (gRNAs) directed against exon IV of genes ATP5G1 and ATP5G2 and exon III of ATP5G3 were identified and optimised with a design tool for CRISPR (clustered regularly interspaced short palindromic repeats; see crispr.mit.edu), synthesised and cloned into the BbsI site of plasmid pSpCas9(BB)-2A-GFP (1) (Addgene). This plasmid encodes the CRISPR associated protein 9 (Cas9) from *Streptococcus pyrogenes* separated from the coding sequence for the green fluorescent protein (GFP) by a 2A sequence. This arrangement leads to GFP being transcribed from the same gene as Cas9, but translated separately from it, allowing cells into which Cas9 has been introduced successfully to be separated and enriched in a fluorescence activated cell sorter. It also expresses the sgRNA consisting of the gRNA fused to a scaffold under the control of the human U6 promoter. The six plasmids (each 0.5 μg) were co-transfected in the presence of lipofectamine 3000 (Thermo Fisher Scientific) into 40-60% confluent HAP1 cells grown in a single well of a six-well plate. Two days later, cells were released with trypsin, and resuspended in IMDM containing 10% (v/v) FBS to a density of 1-2 x 10^6 cells/mL. Green fluorescent cells were separated into single cells in 96 well plates with a High Speed Influx Cell Sorter (BD Biosciences). They were grown at 37^{o}C in the presence of 5% carbon dioxide for 2-3 weeks in IMDM plus 10% FBS until single colonies had formed

in each well. Then they were transferred into 24-well plates, expanded in triplicate, and stored at -80°C in IMDM containing 50% (v/v) FBS and 10% (v/v) dimethylsulfoxide.

Cells in a single well were disrupted for 30 min at room temperature with buffer (100 μL) containing 10 mM Tris.Cl, pH 7.4, 0.2% (w/v) SDS, 1x cOmplete EDTA-free proteinase inhibitor cocktail (Roche) and 0.5 units of benzonase (Merck Millipore). Loading buffer (five times normal concentration) was diluted to normal concentration with the sample, and a portion (10-15 μL) was fractionated on a 10-20% acrylamide gradient protein mini-gel (Thermo Fisher Scientific). Proteins were transferred electrophoretically onto nitrocellulose membranes, and exposed to rabbit antibodies against subunit c (Abcam), and, as loading controls, against Tom20 and the β-subunit of ATP synthase (both Santa Cruz Biotechnology).

The deleted regions of genes were characterized by PCR and DNA sequencing (Source Bioscience). Cells in a single well of a 24-well plate were resuspended in a solution (200 μL) containing 0.2% (w/v) SDS, 75 mM NaCl, 20 mM EDTA and proteinase K (0.4 mg/mL), and the suspension was incubated at 50°C for 2 h. DNA was precipitated with isopropanol, washed with 70% (v/v) ethanol, dried, and redissolved in buffer (100 μL) containing 10 mM Tris.Cl, pH 8.0. The regions containing exons IV of ATP5G1, ATP5G2 and exon III of ATP5G3 were amplified by PCR, and the product sizes analysed by agarose gel electrophoresis. For clone A12, the appropriate PCR fragments were cloned with a TOPO TA Cloning Kit (Thermo Fisher Scientific), and their DNA sequences were determined.

Generation of ρ^0 cells. 143B cells were cultured for ca. 8 weeks as above, but in the presence of ethidium bromide (100 μg/mL) and uridine (100 μg/mL), and then for a further 4-6 passages in the absence of ethidium bromide. The resulting cell line is referred to as 143B-ρ^0. In order to determine that these ρ^0 cells were devoid of mtDNA, total DNA (25 ng) from cells at 90% confluency in a single well was used as a template in real-time PCRs with AmpliTaq Gold DNA polymerase (Applied Biosystems) in an ABI 7900HT Fast Real-Time PCR instrument

with primers and probes for the COXII gene in mitochondrial DNA and the nuclear gene for the amyloid precursor protein (2). A 6-carboxyfluorescein fluorophore and a tetramethylrhodamine quencher (Sigma Genosys) were attached to the 5′ and 3′ ends of the probes, respectively. The mtDNA copy number in HAP1-A12 cells was determined by the same method.

Opening of the PTP. The assays were based on the triggering of opening of the pore by three independent methods. In intact human cells pore opening was induced by thapsigargin (3), or ferutinin (4), and, in cells where the plasma membrane had been permeabilized with digitonin, by examination of the capacity of the mitochondria to retain Ca^{2+} introduced exogenously (5).

Assays with thapsigargin and ferutinin. Mitochondrial membrane potential was monitored via the red fluorescence of tetramethylrhodamine methyl ester (TMRM; excitation and emission wavelengths 530 nm and 675 nm, respectively, with a 75 nm span). In order to follow pore opening, cells were loaded with the acetoxymethyl ester of calcein (calcein-AM), which diffuses into the cells and accumulates in cytosolic compartments, including mitochondria. Once inside cells, esterases remove the acetoxymethyl-group to liberate the green fluorescent calcein molecule, which does not cross the mitochondrial or plasma membranes appreciably during the assay. The fluorescence of cytosolic calcein (excitation and emission wavelengths, respectively of 475 and 560 nm, with a 35 nm span) is quenched by $CoCl_2$, which cannot enter mitochondria and so the fluorescence of mitochondrial calcein is maintained. On triggering pore opening with Ca^{2+}, this green fluorescence is quenched (6). In detail, the assay was performed as follows. Cells were grown to 20-30% confluence in 6-well plates. They were washed three times in modified HBSS buffer (1 mL) consisting of Hanks balanced salt solution (containing Ca^{2+} and Mg^{2+}, with no phenol red, Thermo Fisher Scientific) plus 10 mM HEPES, pH 7.4, 2 mM GlutaMAX supplement (Invitrogen) and 1 mM sodium pyruvate, then kept at room temperature for 20 min in modified HBSS (1 mL) containing 1 μM calcein-AM (Life

Technologies), 25 nM TMRM, and 8 mM $CoCl_2$ (7). They were washed at 37°C three times, each for 5 min, with modified HBSS containing 8 mM $CoCl_2$ (1 mL), and incubated at 37°C in modified HBSS (1 mL) containing 1 mM $CoCl_2$, 20-40 μM thapsigargin or 25 μM ferutinin, for 60 min. When it was employed, the PTP inhibitor CsA (5 μM) was added 5 min before thapsigargin or ferutinin. The concentrations of thapsigargin and CsA were optimised for HAP1 cells (Figs. S10 and S11). In the optimisation of CsA, cyclosporin H (CsH) was used to determine the extent of any possible off-target impact of cyclosporin compounds. CsH is significantly less effective at inhibiting cyclophilin D than CsA (8). The cells were washed twice with modified HBSS buffer (1 mL) containing 1 mM $CoCl_2$ and finally with phosphate buffered saline (PBS; 2 mL) once. The cells were released from monolayers with trypsin and centrifuged (1300xg, 2 min), and the pellet was resuspended in PBS to a concentration of 1-1.5 x 10^6 cells/mL. Nuclei were stained with Hoechst 33342 dye (10 μg/L, final concentration), and the cell suspension was incubated at 37°C for 15 min. The green and red fluorescence intensities of calcein and TMRM, respectively, in cells with or without treatment with thapsigargin or ferutinin were measured in each individual cell in samples of 5000 cells in a Nucleocounter NC3000 cell counting fluorescence microscope (ChemoMetec). The fluorescence intensities of individual cells were plotted on 2D scatter plots, one with the green and blue and the other with red and blue fluorescence intensities on the ordinate and abscissa, respectively. Orthogonal axes were drawn on the control so as to encompass all of the cells that formed a cluster based on their high fluorescence intensities into the upper two quadrants. The axes were placed automatically in the same positions on the experimental scatter plots, and the percentage fraction of cells in each quadrant was recorded by the instrument (see example in Fig. S12). The ratio of the positive percentage (the sums of "the percentage fractions" in the upper two quadrants) from experimentally perturbed and unperturbed control cells is the "relative ratio". The averages of relative ratios from independent duplicate experiments were

plotted on a bar chart. Standard deviations and statistical evaluations by student's t-test were calculated with Excel software.

Capacity of mitochondria to retain calcium. Wild-type HAP1 cells and HAP1-A12 cells were harvested by trypsinization, washed twice in Dulbecco's phosphate buffered saline (DPBS, minus $Ca^{2+}$and Mg^{2+}). They were stained with trypan blue, and counted with a Countess-II FL automated instrument (Thermo Fisher Scientific). Cells were suspended at a concentration of 20 x 10^6/ml in DPBS containing 2x cOmplete EDTA-free protease inhibitor cocktail (Roche), 20 μM EGTA and digitonin (Calbiochem) to 60 μg/ml, and left on ice for 10 min. The resulting permeabilized cells were washed twice with DPBS containing 1x cOmplete inhibitors. Portions of cells (60 x 10^6) required for individual analyses were centrifuged and the cell pellets were kept on ice. Then a portion of the permeabilized cells was re-suspended at 4°C in assay buffer (1 ml) containing 20 mM MOPS-Tris pH 7.2, 120 mM KCl, 10 mM NaCl, 1 mM KH_2PO_4, 5 mM glutamate and 2.5 mM malate. The suspension was diluted 3-fold with assay buffer that had been warmed to 30 °C. Calcium green-5N (0.5 μM) and thapsigargin (1 μM), to prevent Ca^{2+} uptake by the endoplasmic reticulum, were added. If it was intended to inhibit the opening of the pore with CsA (1 μM), it was added during this step. After 2 min, successive portions (10 μl) of 3 mM $CaCl_2$ were added (giving a final concentration 10 μM) with stirring (500 rpm), and the fluorescence of the Calcium green-5N (excitation 505 nm, emission 531 nm) was monitored with a Shimadzu RF-5301PC spectrofluorophotometer. The CsA treated and untreated cells were always assessed in immediate succession in order to make them as comparable as possible. The mitochondrial calcium uniporter was inhibited by the addition of 0.5 μM Ru360 (Calbiochem) immediately after a single Ca^{2+} injection.

Purification of ATP synthase. The procedure was carried out at 4°C. Cells were harvested in PBS containing EDTA-free protease inhibitors (Roche) and total cell protein was estimated by

BCA assay (Thermo Scientific). Mitoplasts were prepared by re-suspension of cells to 5 mg/mL in phosphate buffered saline containing 0.5 mg/mL digitonin, 1 mM dithiothreitol and protease inhibitors (9). After 15 min, they were centrifuged (10,500 x g, 5 min), washed in the same solution lacking digitonin, and extracted with buffer A, pH 8.0, containing 0.1 M Tris, 0.15 M NaCl, glycerol (10% v/v), EDTA-free protease inhibitor, 1-palmitoyl-2-oleoyl-sn-glycero-3-phosphocholine (0.09 mg/mL), 1-palmitoyl-2-oleoyl-*sn*-glycero-3-phosphoethanolamine (0.03 mg/mL), 1-palmitoyl-2-oleoyl-sn-glycero-3-phosphoglycerol (0.03 mg/mL), 2 mM dithiothreitol and digitonin (9 g/g protein). The extract was centrifuged (10,500 x g, 10 min), and the supernatant filtered and stirred for 18 h with an ATP synthase immunocapture resin (Abcam, kit ab109715). The beads were washed in buffer B, differing from buffer A only in the concentration of Tris (20 mM), and the digitonin content (0.05%, w/v). Bound material was eluted in buffer, pH 2.5, containing 0.2 M glycine-HCl and digitonin (0.05%, w/v), and the eluate was neutralised with 1 M Tris.

Mass spectrometric analysis. Stable isotopes were introduced into proteins by stable isotope labelling in cell culture (SILAC). Cells were grown for at least seven doublings in SILAC medium (10) supplemented with proline (200 mg/L), dialysed fetal bovine serum (10%, v/v), penicillin (100 U/mL), streptomycin (100 μg/mL) and either light (R0K0) or heavy (R10K8) isotopes of L-arginine (0.398 mM) and L-lysine (0.798 mM). Each analysis was based on two SILAC experiments one in which the HAP1-A12 cells, or the 143B ρ^0 cells, were labelled in heavy medium and the HAP1 wild-type or the 143B ρ^+ cells in light media, and the second vice versa. Each sample for mass spectrometry consisted of the mitoplast material or ATP synthase purified as above from a 1:1 mixture (based on the protein content) of light and heavy labelled cells (HAP1-A12 and HAP1 wild-type; 143B ρ^0 and 143B ρ^+). Samples were reduced, alkylated and fractionated by SDS-PAGE, and the bands were detected with Coomassie blue dye (11). In-gel tryptic digests (12) of gel slices covering the entire gel track were analysed by

LC-MSMS on a Proxeon EASY-nLC system coupled directly to a LTQ OrbiTrap XL or a Q-Exactive Orbitrap mass spectrometer (ThermoFisher Scientific). Data were processed with MaxQuant version 1.5.0.12 and the integrated Andromeda search engine (13, 14), using a Swiss-Prot human protein database (version July 2016) modified to include mature forms of IF_1 with N-terminal residues Phe-25, Gly-26 and Ser-27 (15, 16), and managed further with Perseus (17). Protein ratios for the various forms of IF_1 were calculated from unique peptides from the import sequence or the N-termini of mature forms, performed manually from the output of the MaxQuant evidence file. The basis of the quantitative experiments using SILAC has been explained before (18).

References

1. Ran FA *et al.* (2013) Genome engineering using the CRISPR-Cas9 system. *Nat Protoc* 8(11):2281–2308.
2. He J *et al.* (2012) Human C4orf14 interacts with the mitochondrial nucleoid and is involved in the biogenesis of the small mitochondrial ribosomal subunit. *Nucleic Acids Res* 40(13):6097–6108.
3. Korge P, Weiss JN (1999) Thapsigargin directly induces the mitochondrial permeability transition. *Eur J Biochem* 265(1):273–280.
4. Abramov AY, Duchen MR (2003) Actions of ionomycin, 4-BrA23187 and a novel electrogenic Ca^{2+} ionophore on mitochondria in intact cells. *Cell Calcium* 33(2):101–112.
5. Murphy AN, Bredesen DE, Cortopassi G, Wang E, Fiskum G (1996) Bcl-2 potentiates the maximal calcium uptake capacity of neural cell mitochondria. *Proc Natl Acad Sci U S A* 93(18):9893–9898.
6. Petronilli V *et al.* (1999) Transient and long-lasting openings of the mitochondrial permeability transition pore can be monitored directly in intact cells by changes in

mitochondrial calcein fluorescence. *Biophys J* 76(2):725–734.

7. Woollacott AJ, Simpson PB (2001) High throughput fluorescence assays for the measurement of mitochondrial activity in intact human neuroblastoma cells. *J Biomol Screen* 6:413–420.
8. Griffiths EJ, Halestrap AP (1991) Further evidence that cyclosporin A protects mitochondria from calcium overload by inhibiting a matrix peptidyl-prolyl cis-trans isomerase. Implications for the immunosuppressive and toxic effects of cyclosporin. *Biochem J* 274 (Pt 2):611–614.
9. Klement P, Nijtmans LG, Van den Bogert C, Houstěk J (1995) Analysis of oxidative phosphorylation complexes in cultured human fibroblasts and amniocytes by blue-native-electrophoresis using mitoplasts isolated with the help of digitonin. *Anal Biochem* 231(1):218–224.
10. Ong SE *et al.* (2002) Stable isotope labeling by amino acids in cell culture, SILAC, as a simple and accurate approach to expression proteomics. *Mol Cell Proteomics* 1(5):376–386.
11. Rhein VF, Carroll J, Ding S, Fearnley IM, Walker JE (2013) NDUFAF7 methylates arginine 85 in the NDUFS2 subunit of human complex I. *J Biol Chem* 288(46):33016–33026.
12. Wilm M *et al.* (1996) Femtomole sequencing of proteins from polyacrylamide gels by nano-electrospray mass spectrometry. *Nature* 379(6564):466–469.
13. Cox J, Mann M (2008) MaxQuant enables high peptide identification rates, individualized p.p.b.-range mass accuracies and proteome-wide protein quantification. *Nat Biotechnol* 26(12):1367–1372.
14. Cox J *et al.* (2011) Andromeda: a peptide search engine integrated into the MaxQuant environment. *J Proteome Res* 10(4):1794–1805.

15. Xu G, Shin SB, Jaffrey SR (2009) Global profiling of protease cleavage sites by chemoselective labeling of protein N-termini. *Proc Natl Acad Sci U S A* 106(46):19310–19315.

16. Vaca Jacome AS *et al.* (2015) N-terminome analysis of the human mitochondrial proteome. *Proteomics* 15(14):2519–2524.

17. Tyanova S *et al.* (2016) The Perseus computational platform for comprehensive analysis of (prote)omics data. *Nat Methods* 13(9):731–740.

18. Cox J, Mann M (2011) Quantitative, high-resolution proteomics for data-driven systems biology. *Annu Rev Biochem* 80:273–299.

A

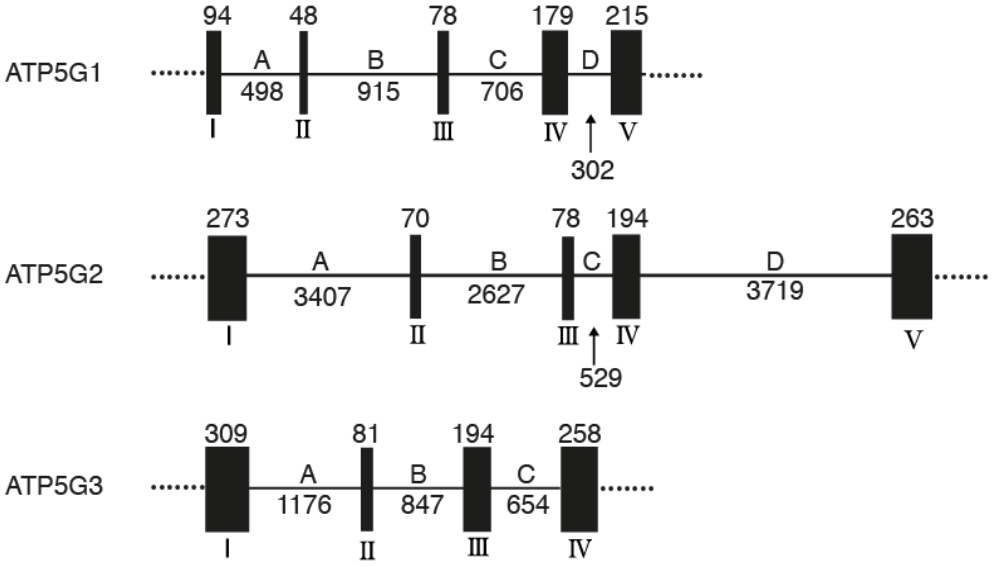

B

```
ATP5G1 MQTAGALFISPALIRCCTRGLIRPVSASFLNSPVNSSKQPSY------SNFPLQVARREF 54
ATP5G2 MFACSKFVSTPSLVKSTSQLLSRPLSAVVLKRPEILTDESLSSL-AVSCPLTSLVSSRSF 59
ATP5G3 MFACAKLACTPSLIRAGSRVAYRPISASVLSRPEASRTGEGSTVFNGAQNGVSQLIQREF 60
       * :.. :  :*:*::. ::   **:** .*. *                    :  *.*

ATP5G1 QTSVVSRDIDTAAKFIGAGAATVGVAGSGAGIGTVFGSLIIGYARNPSLKQQLFSYAILG 114
ATP5G2 QTSAISRDIDTAAKFIGAGAATVGVAGSGAGIGTVFGSLIIGYARNPSLKQQLFSYAILG 119
ATP5G3 QTSAISRDIDTAAKFIGAGAATVGVAGSGAGIGTVFGSLIIGYARNPSLKQQLFSYAILG 120
       ***.:************************************************************

ATP5G1 FALSEAMGLFCLMVAFLILFAM 136
ATP5G2 FALSEAMGLFCLMVAFLILFAM 141
ATP5G3 FALSEAMGLFCLMVAFLILFAM 142
       **********************
```

Fig. S1. Structures of the human ATP5G1, ATP5G2 and ATP5G3 genes and the sequences of the three encoded precursors of the c-subunit of the ATP synthase. A, the genes; exons I-V and introns A-D are represented by solid boxes and continuous lines, respectively. Their sizes are given in base pairs. B, the sequences of the encoded proteins. Only the import sequences are surrounded by blue. Asterisks denote identities.

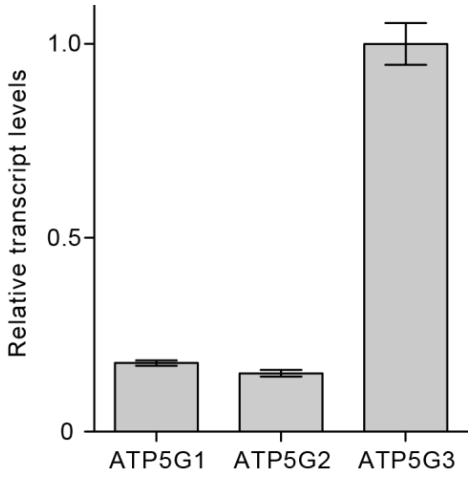

Fig. S2. Transcription of the human genes ATP5G1, ATP5G2 and ATP5G3 in HAP1 cells. The values are normalized to endogenous β-actin and displayed relative to the ATP5G3 transcript, and the error bars show the standard deviations.

Table S1. Target site for gRNA molecules employed in the disruption of the human ATP5G1, ATP5G2 and ATP5G3 genes.

gRNA	Target site
ATP5G1-1	ACAGCAACTTCCCACTCCAG
ATP5G1-2	TGTTTGGCAGCTTGATCATT
ATP5G2-1	GCGCCATTTCAAGGGACATC
ATP5G2-2	CTGGGATTGGAACTGTGTTT

ATP5G3-1	AAGGGAGTTTCAGACCAGTG
ATP5G3-2	GCTGCCAAATTTATTGGTGC

Table S2. Primers employed in the amplification by PCR of the exon targeted by gRNAs in the human ATP5G1, ATP5G2 and ATP5G3 genes.

Primer	Sequence
ATP5G1-Forward	GCAGTTTGCCAACAGTTTCAGAG
ATP5G1-Reverse	GATGAAATCAACCTGAAGGCTCCTG
ATP5G2-Forward	AGGCAAATGCTTCTGAGGCT
ATP5G2-Reverse	GTGCCAGTTTTCCCAGGAGT
ATP5G3-Forward	ATTTGTCTCTTTACACTCAGCTACA
ATP5G3-Reverse	GCTAAGTTTCCAACTACTGCAAGC

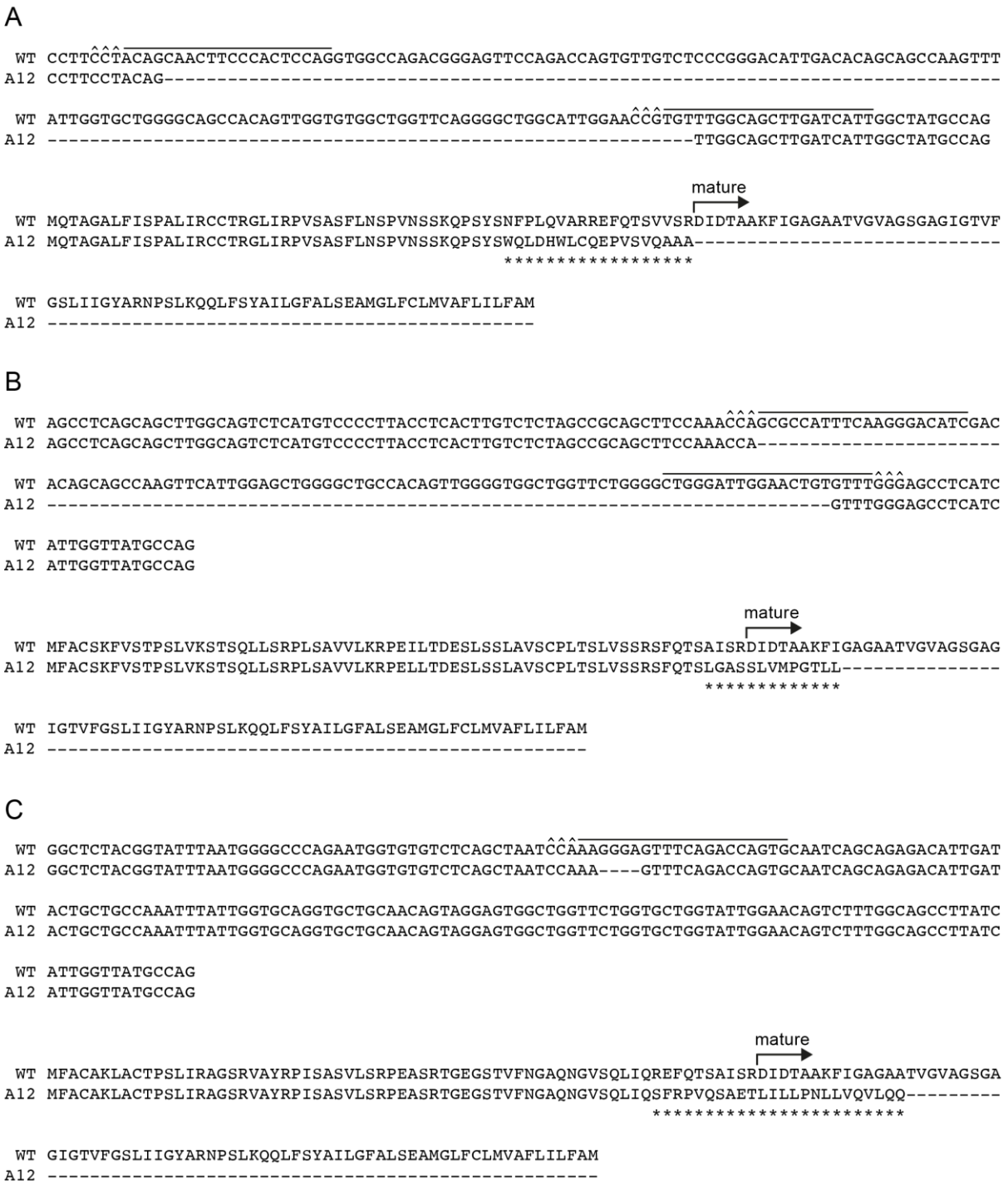

Fig. S3. Deletion of sequences in HAP1 wild-type cells to produce the HAP1-A12 strain. In A-C are shown exons IV of the human ATP5G1 and ATP5G2, and exon III of the ATP5G3 gene, respectively, encoding the subunit c of human ATP synthase. In the upper part of each panel, the sequences of the targeted exon of each gene in the parental or wild-type (WT) cells are aligned with the corresponding deleted sequence in the HAP1-A12 cells. Carets indicate

the PAM (protospacer adjacent motif) sequences for each guide RNA, and solid bars the guide RNA target sequences. In the lower part of A-C, the impacts of the deletions on the sequences of the import precursors of the c-subunit are shown. The start of the mature protein is indicated. Amino acid changes introduced by the process of deletion are indicated by asterisks. Dashed lines indicate deletions in DNA and protein sequences.

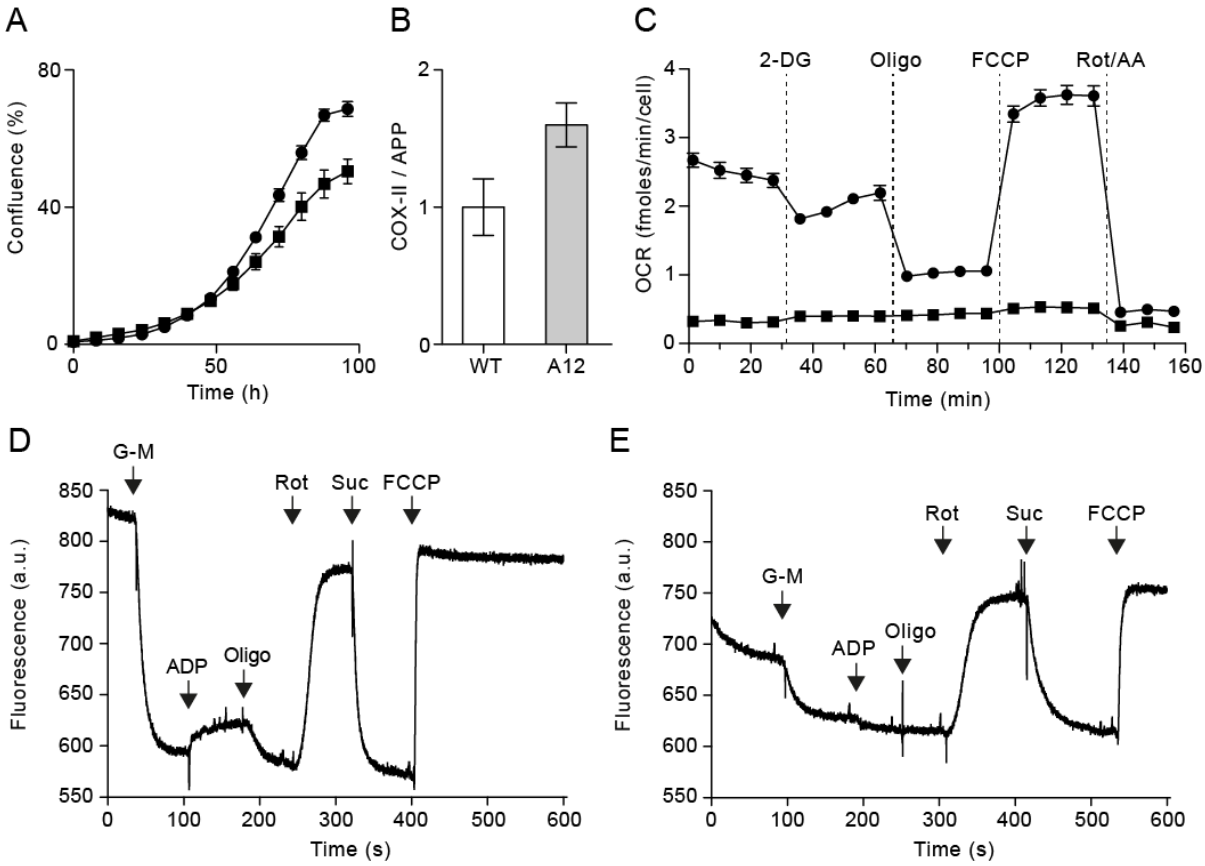

Fig. S4. Characteristics of HAP1-A12 cells. In A and C, ●, HAP1 wild-type cells; ■, HAP1-A12 cells. A, growth rates of HAP1 cells. About 40,000 cells were seeded into individual wells of a 6-well plate, and their confluence was monitored over 96 h. The data points are the mean values ±SD (n=3); B, the relative copy numbers of mtDNA in HAP1 cells. Regions of the genes for COX II and the amyloid precursor protein (APP) were amplified and quantitated as indices of mitochondrial and nuclear DNA, respectively. All data are the mean values ±SDs (n=4); C, cellular oxygen consumption rates (OCR) before and after sequential additions of 2-

deoxyglucose (2-DG), oligomycin (Oligo), carbonyl cyanide-4-(trifluoromethoxy)phenylhydrazone (FCCP), and a mixture of rotenone and antimycin A (Rot/AA), at the times indicated. Data represent the mean ±SEM (n=8 or 9 wells). D and E, TMRM fluorescence measurements with permeabilized wild-type HAP1 and HAP1-A12 cells, respectively, normalized to zero after the addition of succinate and to 1 following FCCP treatment; 5 mM glutamate and 2.5 mM malate (G-M), 0.1 mM ADP; 1 μM oligomycin (Oligo), 1 μM rotenone (Rot), 10 mM succinate (Suc), and 1 μM FCCP were added as indicated.

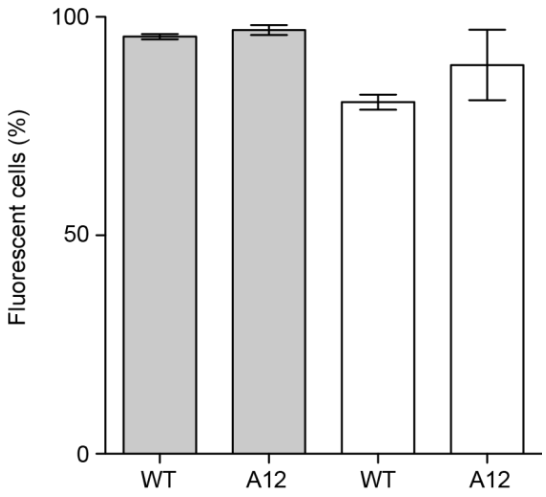

Fig. S5. Comparison of the efficiency of staining of HAP1 wild-type cells and HAP1-A12 cells by calcein and TMRM. Grey and white histograms correspond to cells stained with calcein and/or TMRM, respectively. The percentage of fluorescent cells was determined with a Nucleocounter 3000. All data are the mean values ± SDs (n=4).

Table S3. Number of calcium pulses recorded in permeabilized wild-type HAP1 cells.

The values in the first row refer to Fig. 4A and 4B. Rows 2-9 correspond to replicate experiments.

No CsA	With CsA	Ratio
7	20	2.86
6	26	4.33
5	13	2.6
11	25	2.27
7	21	3.0
11	30	2.86
7	21	3.0
7	21	3.0
5	11	2.2
Av. 7.3	Av. 20.9	Av. 2.89
SD. 2.2	SD. 6.0	SD. 0.62

Table S4. Number of calcium pulses recorded in permeabilized HAP1-A12 cells.

The values in the first row refer to Fig. 4D and 4E. Rows 2-4 correspond to replicate experiments.

No CsA	With CsA	Ratio
8	21	2.63
14	40	2.86
9	18	2.0
7	17	2.43

Av. 9.5	Av. 24.0	Av. 2.48
SD. 3.1	SD. 10.8	SD. 0.36

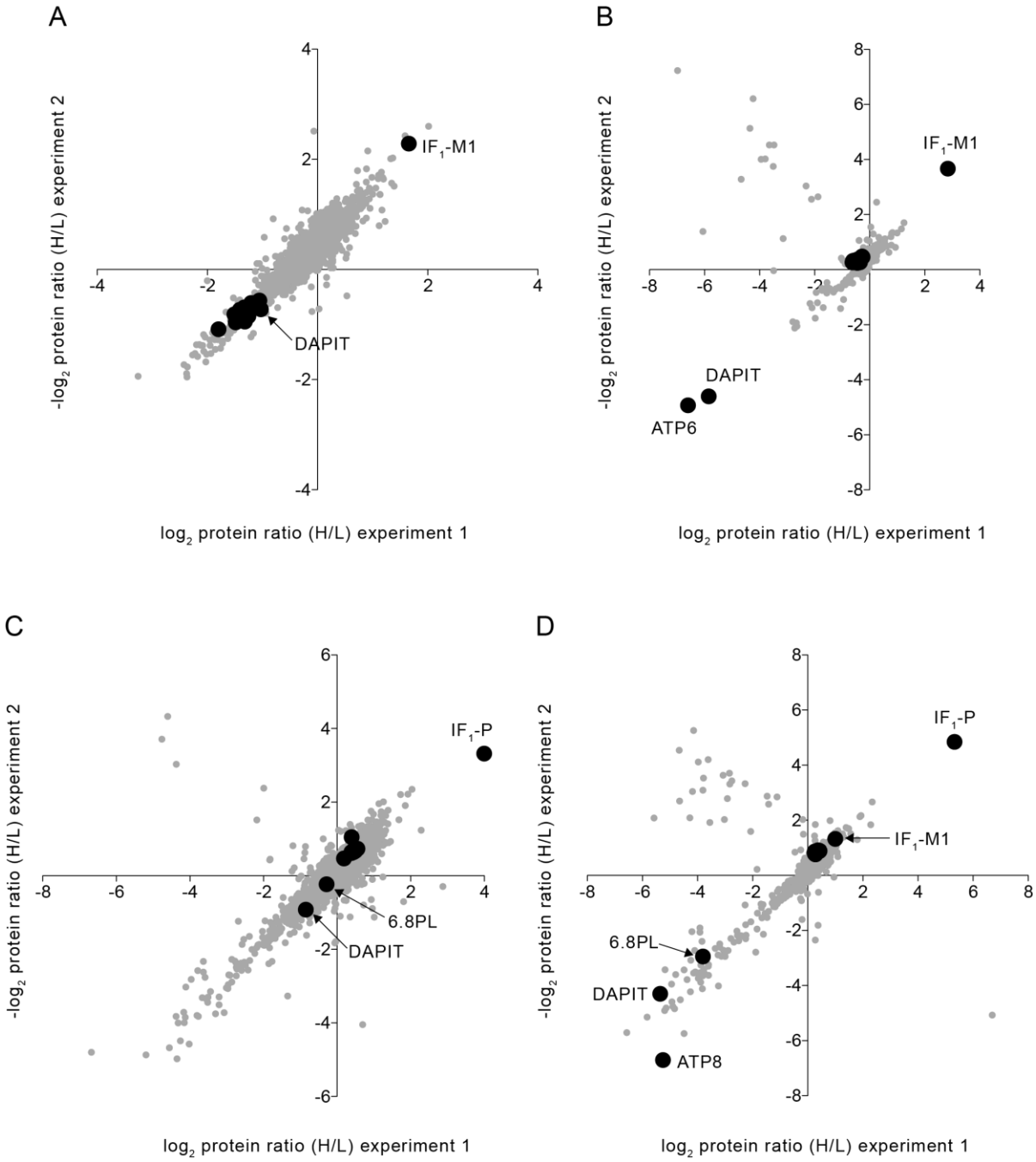

Fig. S6. Effects on protein relative abundance of the deletion of the c-subunit of human ATP synthase in HAP1 cells, and of the removal of ATP6 and ATP8 in 143B ρ^0 cells. Relative

quantitative mass spectrometry analyses of proteins in mitoplasts (parts A and C) and purified ATP synthase (parts B and D) prepared from a 1:1 mixture of cells that were differentially SILAC-labelled. Panels A and B show the analyses of wild-type HAP1 cells combined with HAP1-A12 cells devoid of the ATP synthase c-subunit, and C and D the data from wild-type 143B ρ^+ cells and ρ^0 cells lacking mitochondrial DNA. The experiments were performed twice, using reciprocal SILAC labelling orientations. For all the scatter plots each data point corresponds to the relative abundance ratio of an identified protein from the two complementary labelling experiments. ●, ATP synthase subunits and the precursor (P), or the M1 mature form of IF_1; ●, all other identified proteins. Protein ratios and peptide evidence for IF_1 are listed in Tables S5 to S12.

A

```
          *       10          20          30          40          50          60
IF1-P     MAVTALAARTWLGVWGVRTMQARGFGSDQSENVDRGAGSIREAGGAFGKREQAEEERYFR
IF1-M1                               FGSDQSENVDRGAGSIREAGGAFGKREQAEEERYFR
IF1-M2                                GSDQSENVDRGAGSIREAGGAFGKREQAEEERYFR
```

B

```
          *       10          20          30          40          50          60
   f-1    MASVGECPAPVPVKDKKLLEVKLGELPSWILMRDFSPSGIFGAFQRGYYRYYNKYINVKK
   f-2    MASV------VPVKDKKLLEVKLGELPSWILMRDFSPSGIFGAFQRGYYRYYNKYINVKK

                  70          80          90
   f-1    GSISGITMVLACYVLFSYSFSYKHLKHERLRKYH
   f-2    GSISGITMVLACYVLFSYSFSYKHLKHERLRKYH
```

Fig. S7. Sequences of the precursor and mature forms of the inhibitor protein IF_1 and isoforms of subunit f of the human mitochondrial ATP synthase. The asterisks denote that the initiator methionine residue has been removed, and residue alanine-2 has been Nα-acetylated. A, residues 1-60 of the initial precursor form of IF_1 (top line) and formation of IF_1-P, and below the observed mature forms IF_1-M1 and IF_1-M2; B, complete sequences of isoforms f-1 and f-2. They arise by an alternative splicing mechanism, and differ in the region denoted by shading

and dashes. Both isoforms were observed in mass spectrometric analyses. Subunit f lacks a processed N-terminal mitochondrial import sequence.

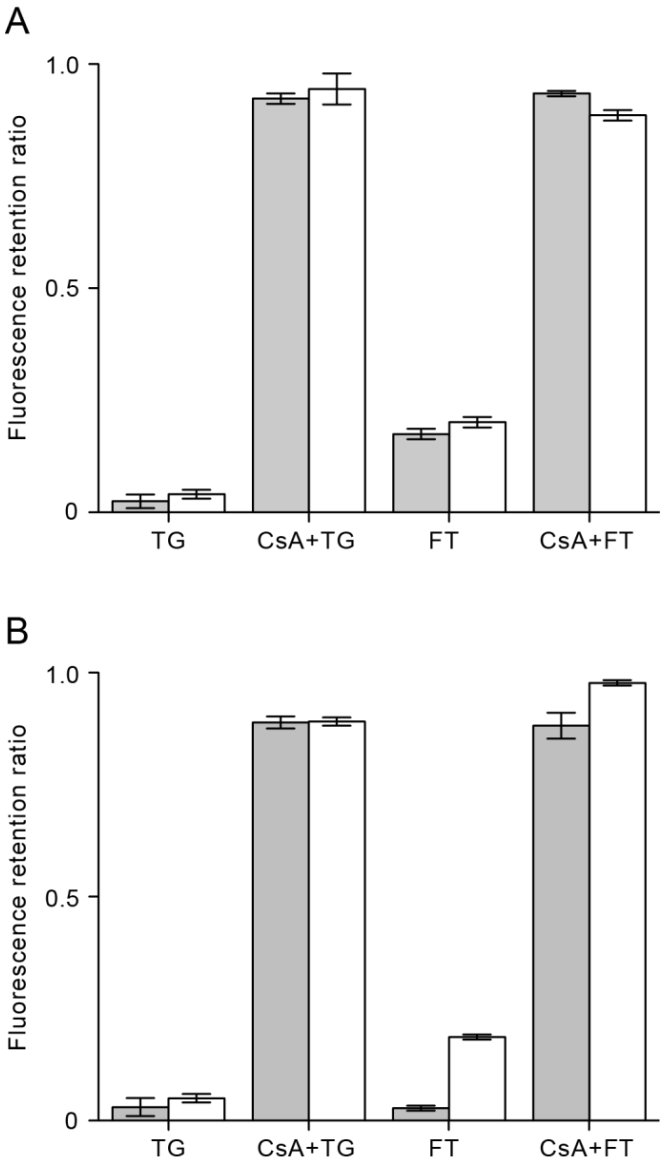

Fig. S8. Presence of the PTP in human 143B cells. A, and B, ρ^+ and ρ^0 cells. Retention ratios in 143B cells for calcein (grey) and TMRM (white). The cells were treated with 20 μM thapsigargin (TG) or 25 μM ferutinin (FT) for 1 h, respectively, with or without CsA (5 μM). TG activated cells were treated with CsA before staining whereas the FT cells were stained

with calcein and TMRM, and then treated with CsA. All ratios were normalized to the untreated 143B cells (loaded with DMSO vehicle). The data represent means ± SDs (TG, n=4; FT, n=2).

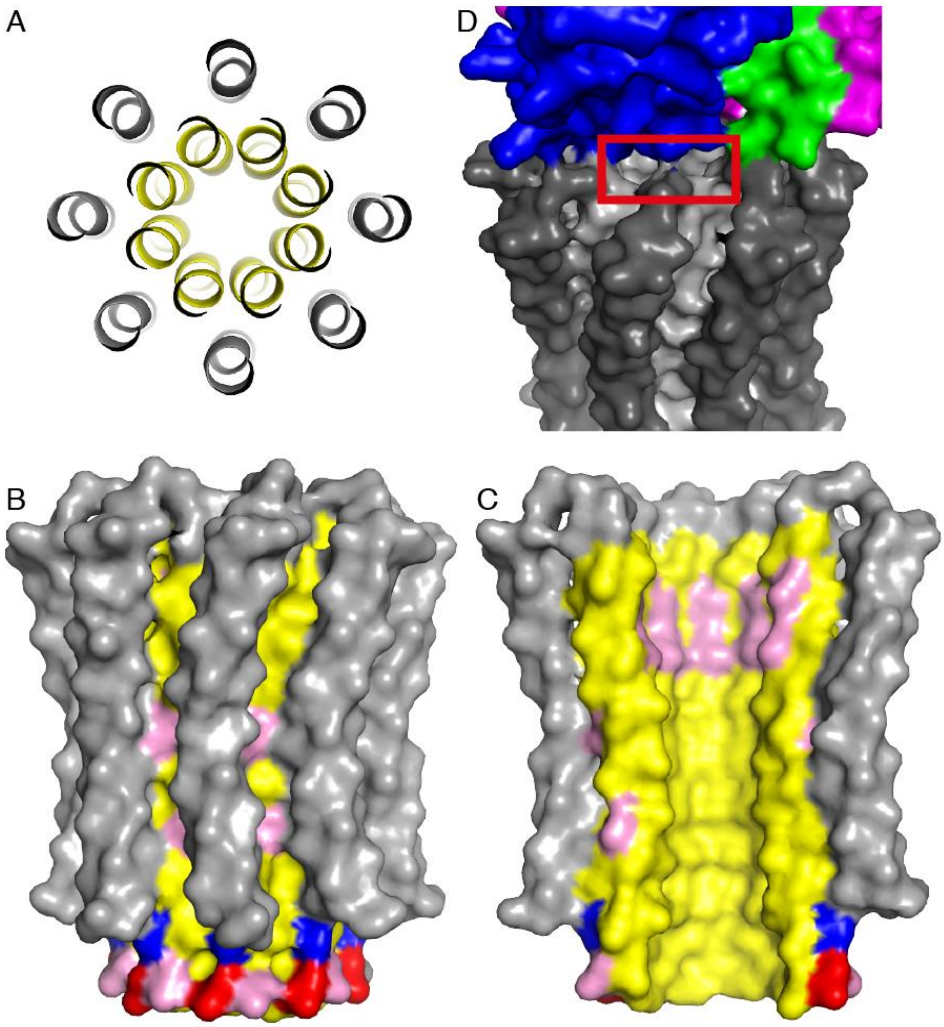

Fig. S9. Structure of the c_8-ring from bovine ATP synthase. As the sequences of the bovine and human c-subunits are the same, the structures of their c_8-rings are identical. A, cross-section of the ring showing concentric annuli of N- and C-terminal transmembrane α-helices; B, external view of the surface of the intact ring (inner and outer yellow and grey rings, respectively); C, internal view of the surface of half of the ring (four c-subunits). In the inner ring, yellow, pink, red and blue regions denote hydrophobic, hydrophilic, basic and acidic

residues, respectively; D, view of the region of contact between the c_8-ring (below) and foot of the central stalk, in the enzyme's rotor. Blue, green and magenta areas are parts of the γ-, δ- and ε-subunits. The c_8-ring is grey. The red box indicates a small crevice in the model at 3.5 Å resolution leading to the central cavity. In reality, the crevice is probably occupied by the side chains of amino acids, which were truncated at the β-carbon atom in the model.

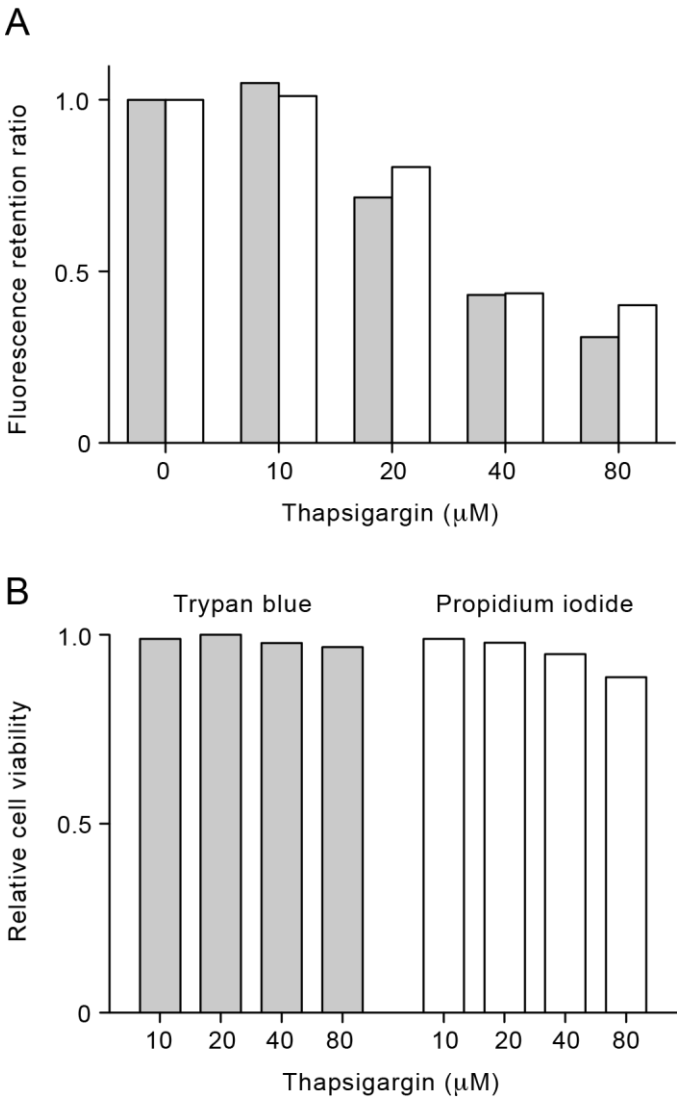

Fig. S10. Optimisation of thapsigargin concentrations on the opening of the PTP in wild-type HAP1 cells. A, the cells were stained with both calcein and TMRM, then incubated for 1 h with various concentrations of thapsigargin. Grey and white columns represent the retention ratios for calcein and TMRM fluorescence signals, respectively, relative to untreated cells. B,

HAP1 cell viability after treatment with thapsigargin for 1 h was assessed by both trypan blue and propidium iodide staining, with a Countess-II FL automated cell counter (Thermo Fisher Scientific) or a NC3000 advanced image cytometer (ChemoMetec), respectively. The values are expressed relative to untreated HAP1 cells.

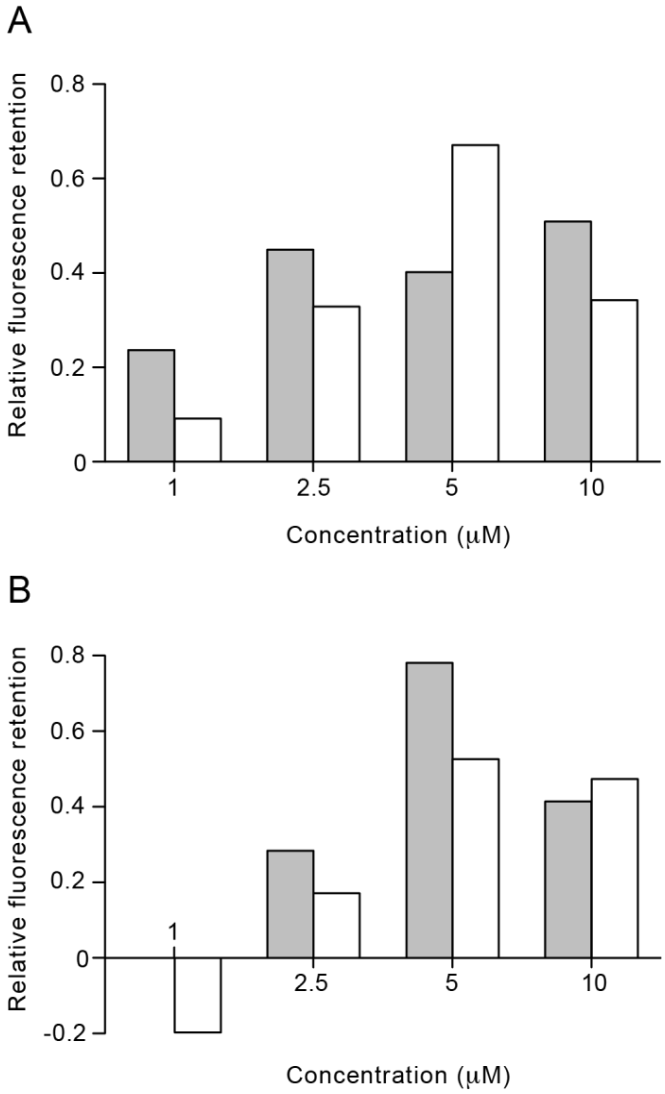

Fig. S11. Cyclosporin A concentration dependent inhibition of the PTP in wild-type HAP1 cells. Cells were stained with both calcein and TMRM, then pre-incubated with different concentrations of CsA or CsH for 5 min, and then treated for 1 h with 40 μM thapsigargin (A) or 25 μM ferutinin (B). The fluorescence retention ratio for calcein and TMRM was determined, relative to untreated cells. Grey and white columns difference values (CsA minus

CsH) for calcein and TMRM fluorescence signals, respectively.

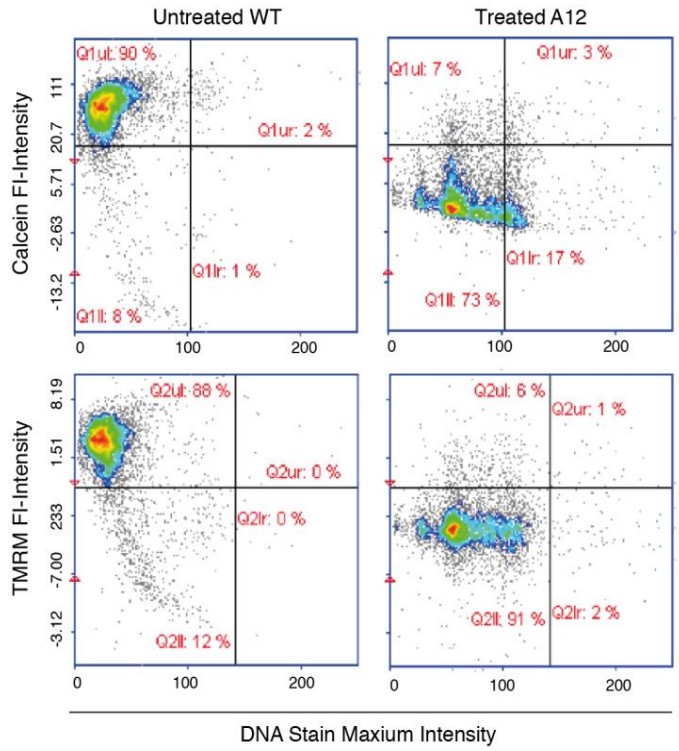

Fig. S12. An example of scatter plots used in the assay of the PTP. HAP1-A12 (A12) and HAP1 wild-type (WT) cells were stained with both calcein and TMRM. Then both sets of cells were incubated for 1 h in the presence of 25 µM ferutinin (FT) or DMSO vehicle, respectively. Green and red fluorescence intensities of calcein and TMRM, respectively, of samples of 5000 cells with or without treatment with ferutinin were measured in a Nucleocounter NC3000 cell counting fluorescence microscope (ChemoMetec). Then, orthogonal axes were drawn manually on the 2D scatter plots for the WT cells and then used as the master template for the scatter plots for the HAP1-A12 cells. The relative calcein retention ratio was calculated as the ratio of HAP1-A12 positive percentages (the sum of the two percentages in the upper quadrants for A12: 7+3%=10%) and the positive percentages for wild-type cells (WT) (the sum of the

two percentages in the corresponding upper quadrants: 90+2%=92%). The values of intensities on both axes should be multiplied by 10^3.

Supplementary Table S5. Proteins identified in SILAC experiments comparing immunopurifed ATP synthase from wild-type and HAP1-A12 cells.

Supplementary Table S6. Peptide data for the ATPase inhibitor protein obtained in SILAC experiments comparing ATP synthase from wild-type and HAP1-A12 cells.

Supplementary Table S7. Proteins identified in SILAC experiments comparing immunopurified ATP synthase from wild-type and 143B ρ^0 cells.

Supplementary Table S8. Peptide data for the ATPase inhibitor protein obtained in SILAC experiments comparing ATP synthase from wild-type and ρ^0 143B cells.

Supplementary Table S9. Proteins identified in SILAC experiments comparing mitoplasts from wild-type and HAP1-A12 cells.

Supplementary Table S10. Peptide data for the ATPase inhibitor protein obtained in SILAC experiments comparing mitoplasts from wild-type and HAP1-A12 cells.

Supplementary Table S11. Proteins identified in SILAC experiments comparing mitoplast material from wild-type and 143B ρ^0 cells.

Supplementary Table S12. Peptide data for the ATPase inhibitor protein obtained in SILAC experiments comparing mitoplasts from wild-type and 143B ρ^0 cells.